Optimal Control of Connected Vehicle Systems With Communication Delay and Driver Reaction Time

Jin I. Ge and Gábor Orosz

***Abstract*— In this paper, linear quadratic regulation is used to obtain an optimal design of connected cruise control (CCC). We consider vehicle strings where a CCC vehicle receives position and velocity signals through wireless vehicle-to-vehicle communication from multiple vehicles ahead. Communication delay, driver reaction time, and heterogeneity of vehicles are considered. The optimal feedback law is obtained by minimizing a cost function defined by headway and velocity errors and the acceleration of the CCC vehicle on an infinite horizon. We show that, by decomposing the optimization problem, the feedback gains can be obtained recursively as signals from vehicles farther ahead become available, and that the gains decay exponentially with the number of cars between the source of the signal and the CCC vehicle. Such properties allow graceful degradation of CCC performance under imperfect communication. The effects of the cost function on the head-to-tail string stability are also investigated and the robustness against variations in human parameters is tested. The analytical results are verified by numerical simulations at the nonlinear level. The results allow us to significantly reduce the complexity of CCC design.**

***Index Terms*— Connected vehicles, delay systems, optimal control.**

I. Introduction

SINCE the invention of the automobile over a century ago, automotive engineers have been trying to improve safety and passenger comfort and provide higher level of mobility for customers. However, during the past decades the level of traffic congestion has become a bottleneck for mobility, while stop-and-go traffic significantly impacts the fuel economy of vehicles [1]. Therefore, for sustainable road transportation, it is not adequate to simply improve the performance of individual cars, but their impact on traffic flow also needs to be evaluated. Although improving the infrastructure may alleviate traffic congestion, we may design better controllers for individual vehicles, and use these agents to 'steer' the traffic flow as a multi-agent system towards more desired states. In this paper we focus on the latter strategy.

Manuscript received February 1, 2016; revised June 10, 2016, July 30, 2016, and September 18, 2016; accepted November 16, 2016. Date of publication December 12, 2016; date of current version July 31, 2017. This work was supported by the National Science Foundation under Award 1351456. The Associate Editor for this paper was H. A. Rakha.

The authors are with the Department of Mechanical Engineering, University of Michigan, Ann Arbor, MI 48109 USA (e-mail: gejin@umich.edu; orosz@umich.edu).

Color versions of one or more of the figures in this paper are available online at http://ieeexplore.ieee.org.

Digital Object Identifier 10.1109/TITS.2016.2633164

One primary factor under consideration is the longitudinal control of vehicle motion. Since human drivers have relatively large reaction time and limited perception abilities, they often perform poorly as controllers for the vehicle. Using adaptive cruise control (ACC), one may improve the longitudinal control due to faster and more accurate sensing abilities and more sophisticated control strategies [2], [3]. However, the range sensors (radar, lidar) used for ACC are quite expensive and the penetration rate of ACC systems has not increased significantly over the last couple of years. Moreover, ACC cannot overcome the limitation that only motion information of the vehicle immediately ahead can be monitored by range sensors. This restricts the performance of the cruise controller and limits our ability to improve the traffic flow.

Therefore, researchers proposed to utilize motion information about the traffic environment around the vehicle using wireless vehicle-to-infrastructure (V2I) and vehicle-to-vehicle (V2V) communication [4], [5]. In this case, vehicles may be controlled while taking into account traffic flow conditions over a longer spatial horizon. Previous strategies included cooperative adaptive cruise control (CACC) where a fixed communication structure is assigned to a group of ACC vehicles, so that a platoon could run with relatively small headway, while velocity fluctuations are attenuated as propagating backwards along the vehicle chain [6]–[9]. Various application scenarios have been discussed for CACC, with the focus on designated-lane highway driving [10]–[12]. Some researchers are trying to loosen the rigid requirement on communication topology for CACC, so that it may deal with more realistic multi-vehicle formations [13]–[15]. However, such cooperative systems often rely on existing ACC systems, and thus may be limited in real-traffic implementation.

In [16] and [17] connected cruise control (CCC) was proposed to maintain smooth traffic flow in mixed systems of conventional, ACC, and communication-assisted vehicles. The CCC controller receives information about the motion of multiple vehicles ahead, and actuates the vehicle or assists the driver based on these signals. The controller may include any signals available and thus allow various connectivity topologies to form among CCC and non-CCC vehicles. The influence of connectivity structures, signal types, packet drops, and communication delays on the longitudinal dynamics of vehicular chains has been investigated in [17]–[21]. By tuning the corresponding control gains one may ensure desired performance, such as plant stability (the ability to maintain

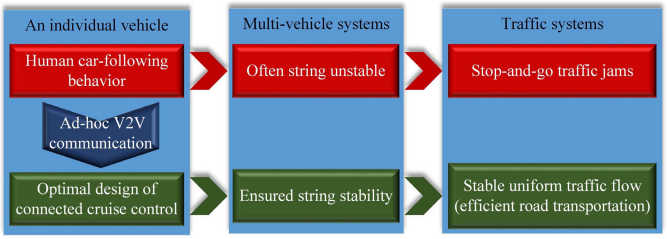

Fig. 1. Functional scheme of the optimal connected cruise control design

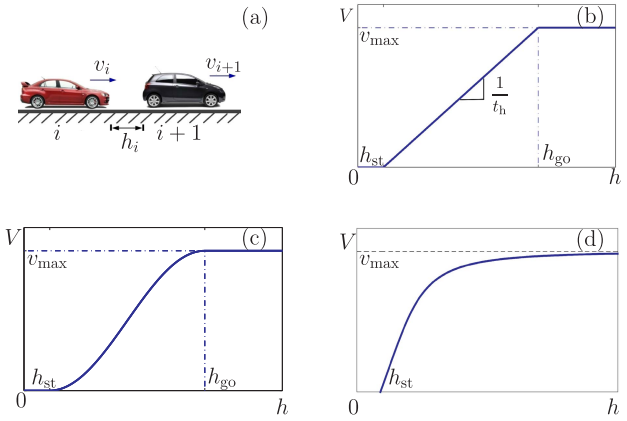

Fig. 2. (a): Single-lane car-following of human-driven vehicles showing the headway and the velocities. (b): The range policy (3,4) used in the literature, where $v_{\max}$ is the maximum velocity allowed for the vehicle, $h_{\rm st}$ is the smallest headway before the vehicle intends to stop, and $h_{\rm go}$ is the largest headway after which the vehicle intends to maintain $v_{\max}$. (c): The range policy (3,5) used in this paper. (d): The range policy (8) implicitly contained in the IDM.

chosen speed without external perturbations) and string stability (the suppression of velocity fluctuations along the vehicular chain). These may have a positive impact on the performance of the whole transportation system as emphasized by the diagram in Fig. 1.

However, optimality of control gains in terms of minimizing velocity fluctuations has not yet been discussed for large connected vehicle systems. Optimal CACC designs often use algorithms with relatively high computational cost, such as rolling horizon optimal control [14], which is only feasible when considering a small group of vehicles with specific communication structures. Thus, it is necessary to find optimization algorithms with low computational cost for more general connectivity topologies. While [22] presented some initial ideas about low-cost optimal design, driver reaction time and communication delay were not considered. Here we present an algorithm that is compatible with human car-following behaviors while still allowing us to fully exploit the connectivity without increasing the complexity of gain-tuning.

In this paper we optimize the gains of a CCC vehicle that receives position and velocity information from multiple human-driven vehicles ahead using linear quadratic regulation (LQR). The controller design is based on the minimization of velocity and headway fluctuations and the control cost (acceleration/deceleration) for the CCC vehicle. We use optimization as a tool to observe different levels of reliance on various signals and apply the findings in CCC design. While the optimization is performed over a high-dimensional network, we show that the problem can be decomposed since the information flow is uni-directional in a connected vehicle system when vehicles only utilize motion information of vehicles ahead. Such decomposition allows us to obtain an analytical solution to the optimization problem recursively, and it allows graceful degradation of CCC performance when V2V communication deteriorates. We also show that the weights in the cost function can be chosen such that the velocity fluctuations of the CCC vehicle are attenuated compared with vehicles ahead (i.e., string stability can be achieved). While the optimization is done at the linear level, we demonstrate that the controller performs well at the nonlinear level, and is robust against parameter variations and heterogeneities appearing in multi-vehicle systems.

The layout of this paper is as follows. In Section II we present models for human driving and build up the models for CCC design. In Section III we introduce the setup of the optimization problem and show that the solution of an infinite-dimensional Riccati equation can be used to design the CCC controller. The details for solving the optimization problem with time delay and the robustness of the proposed controller are provided in the Appendix for interested readers. In Section IV we present the stability analysis and summarize the impact of design parameters and robustness against variations in human parameters using stability charts. In Section V the application of the CCC controller is demonstrated at the nonlinear level using numerical simulations. Finally, we conclude and lay out some future research directions in Section VI.

II. Modeling the Car-Following Behavior

In this section we model the car-following behavior of both human drivers and the CCC controller in non-emergency situations. Since we are concerned with longitudinal motion control of vehicles, we consider single-lane car-following models of human-driven vehicles; see Fig. 2(a).

Many models exist in the literature, as summarized in [23] and [24]. These include continuous-time ones like the intelligent driver model (IDM) [25], the optimal velocity model (OVM) [26], the GM model [27], [28], the Pipes model [29], and discrete-time ones like the Krauss model [30] and the Wiedemann model [31]. Over the past decades many variations of these models have been developed in the efforts to reproduce a wide range of traffic phenomena by computer simulation [32], [33]. While models using a large number of parameters may be considered to be of higher fidelity, difficulties in parameter estimation through data fitting may negatively affect their accuracy [34], [35].

Thus we consider a class of continuous-time car-following models with a few parameters that include driver reaction time delay. These models (e.g., OVM, IDM, and GM model) can

be written in the form

$$\dot{h}_i(t) = v_{i+1}(t) - v_i(t)\,,$$
$$\dot{v}_i(t) = F\big(h_i(t-\tau), \dot{h}_i(t-\tau), v_i(t-\tau)\big)\,, \qquad (1)$$

to describe the car-following behavior of vehicle i. Here the dot stands for differentiation with respect to time t, τ is the human reaction time delay, h_i denotes the headway, i.e., the bumper-to-bumper distance between vehicle i and its predecessor, and v_i denotes the velocity of vehicle i; see Fig. 2(a). Here we provide some details about the OVM and the IDM that are used very frequently in the literature. However, we remark that the controller design applied in this paper is applicable to any model of the form (1).

In case of the OVM [18], the vehicle acceleration is determined by the difference between the headway-dependent desired velocity and the actual velocity and by the velocity difference between the vehicle and its predecessor, that is

$$F(h, \dot{h}, v) = \alpha\big(V(h) - v\big) + \beta\dot{h}\,, \qquad (2)$$

where the gains α and β are used by the human drivers to correct velocity errors. The desired velocity is determined by the headway using the continuous range policy

$$V(h) = \begin{cases} 0 & \text{if} \quad h \le h_{\rm st}\,, \\ f_{\rm v}(h) & \text{if} \quad h_{\rm st} < h < h_{\rm go}\,, \\ v_{\max} & \text{if} \quad h \ge h_{\rm go}\,, \end{cases} \qquad (3)$$

i.e., the desired velocity is zero for small headways ($h \le h_{\rm st}$) and equal to the maximum speed $v_{\max}$ for large headways ($h \ge h_{\rm go}$). Between these, the desired velocity is given by $f_{\rm v}(h)$ which increases with the headway monotonically. There are many choices for the specific function of $f_{\rm v}(h)$, but the qualitative dynamics remain similar if the above characteristics are kept [18], [19]. In [12] the function

$$f_{\rm v}(h) = v_{\max}\frac{h - h_{\rm st}}{h_{\rm go} - h_{\rm st}} \qquad (4)$$

was used, which corresponds to the constant time headway $t_{\rm h} = (h_{\rm go} - h_{\rm st})/v_{\max}$, as shown in Fig. 2(b). However, the range policy (3,4) is non-smooth at $h = h_{\rm st}$ and $h = h_{\rm go}$ and may generate a "jerky ride". Thus, here we use

$$f_{\rm v}(h) = \frac{v_{\max}}{2}\left(1 - \cos\left(\pi\,\frac{h - h_{\rm st}}{h_{\rm go} - h_{\rm st}}\right)\right) \qquad (5)$$

as shown in Fig. 2(c). The range policy (3,5) is smooth but has a changing time headway given by $t_{\rm h} = 1/f_{\rm v}'(h)$.

We assume that human-driven vehicles try to maintain the uniform traffic flow equilibrium

$$h_i(t) \equiv h^*\,, \quad v_i(t) \equiv v^*\,, \qquad (6)$$

given by $F(h^*, 0, v^*) = 0$, cf. (1). Using (2) we find the equilibrium speed-headway relation of OVM given by its range policy function (3), i.e., $v^* = V(h^*)$.

On the other hand, the IDM [25] can be written in the form

$$F(h, \dot{h}, v) = a\left(1 - \left(\frac{v}{v_{\max}}\right)^4 - \left(\frac{h_{\rm st} + T_{\rm gap}v - \dot{h}v/\sqrt{4ab}}{h}\right)^2\right), \qquad (7)$$

where a is the maximum desired acceleration, $T_{\rm gap}$ is the desired time gap, and b is the comfortable acceleration. While (7) does not contain a range policy function explicitly, the equilibrium speed-headway relation

$$h^* = V^{-1}(v^*) = \frac{h_{\rm st} + T_{\rm gap}v^*}{\sqrt{1 - (v^*/v_{\max})^4}}\,, \qquad (8)$$

shown in Fig. 2(d), describes qualitatively the same driving behavior as in Fig. 2(b,c). Notice that for $h^* < h_{\rm st}$, we have $v^* < 0$ in the IDM, which can be eliminated by requiring vehicle velocities to be non-negative.

Observe that both the OVM (1,2) and the IDM (1,7) can be linearized into the same form [18]. Here we use the particular form (2) when performing the linearization (as the parameters α and β have clear physical meaning), but all results can be generalized for an arbitrary $F(h, \dot{h}, v)$. By assuming the system in the vicinity of the equilibrium (6) and defining the headway and velocity perturbations

$$\tilde{h}_i(t) = h_i(t) - h^*, \quad \tilde{v}_i(t) = v_i(t) - v^*\,, \qquad (9)$$

we linearize (1,2) to obtain the linear delay differential equation (DDE)

$$\dot{\tilde{h}}_i(t) = \tilde{v}_{i+1}(t) - \tilde{v}_i(t)\,,$$
$$\dot{\tilde{v}}_i(t) = \alpha\big(N^*\tilde{h}_i(t-\tau) - \tilde{v}_i(t-\tau)\big) + \beta\big(\tilde{v}_{i+1}(t-\tau) - \tilde{v}_i(t-\tau)\big). \qquad (10)$$

Here $N^* = V'(h^*)$ is the derivative of the range policy (3) at the equilibrium, and for $h_{\rm st} \le h^* \le h_{\rm go}$ this gives the time headway $t_{\rm h} = 1/f_{\rm v}'(h^*) = 1/N^*$.

Controllers with a small time headway produce more aggressive car-following behaviors, which makes it more difficult to maintain uniform traffic flow [36]. Based on highway traffic data [18], we set $v_{\max} = 30$ [m/s], $h_{\rm st} = 5$ [m], $h_{\rm go} = 35$ [m]. We find at $v^* = 15$ [m/s], $h^* = 20$ [m] the range policy (3,5) has the largest derivative $N^* = \pi/2$ [1/s] and correspondingly the smallest time headway $t_{\rm h} \approx 0.64$ [s]. We consider this least-string-stable operating point in the remainder of this paper.

We now consider the single-lane configuration shown in Fig. 3 where the CCC vehicle at the tail receives position and velocity signals of the n non-CCC vehicles ahead through V2V communication (see dashed arrows from preceding vehicles to vehicle 1). Initially, we assume that all preceding vehicles are identical human-driven vehicles, but the effects of heterogeneous dynamics among preceding vehicles will be investigated in Appendix D.

The car-following dynamics of the CCC vehicle is given by

$$\dot{h}_1(t) = v_2(t) - v_1(t)\,,$$
$$\dot{v}_1(t) = u(t)\,, \qquad (11)$$

where $u(t)$ is the acceleration that will be designed using the velocity and headway information obtained via V2V communication. Communication delay is not included explicitly in the optimization, but will be added when analyzing the stability of CCC in Section IV.

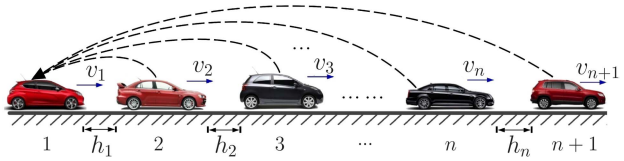

Fig. 3. A string of $n+1$ vehicles in a single-lane scenario. The CCC vehicle at the tail receives signals from human-driven vehicles ahead via V2V communication. Dashed arrows indicate the flow of information in this connected vehicle system.

We assume the CCC vehicle tries to maintain the same equilibrium as human-driven vehicles $i = 2, \ldots, n$, cf. (6). Using definition (9) we linearize (11) about the equilibrium:

$$\begin{aligned} \dot{\tilde{h}}_1(t) &= \tilde{v}_2(t) - \tilde{v}_1(t)\,, \\ \dot{\tilde{v}}_1(t) &= u(t)\,. \end{aligned} \tag{12}$$

With the car-following dynamics of human-driven and CCC vehicles set up, we discuss how to use optimization to design $u(t)$ in Section III.

III. Connected Cruise Control Design Using Linear Quadratic Regulation

In this section, we present a systematic method for connected cruise control design while utilizing the linearized human car-following model (10). In Section III-A we present the linear quadratic optimization setup for CCC design that exploits V2V information broadcasted by human-driven vehicles ahead. In Section III-B we present the general solution of the optimization problem, while in Section III-C we show that the problem can be decomposed and solved analytically by exploiting the unidirectional information flow in the system. If the reader is not interested in these technical details, Sections III-B and III-C may be skipped. In Section III-D we obtain the CCC controller with full-state feedback and demonstrate that the gains decay exponentially as the number of vehicles between the source and the CCC vehicle increases. We also show that adding more vehicles downstream does not influence the existing design for the system. A brief discussion is provided in Appendix D on the robustness of the controller against heterogeneities arising in the vehicle string.

A. Optimization Problem Setup

Here we formulate the CCC design as a linear quadratic (LQ) optimization problem with delay. Since the CCC vehicle would like to maintain constant velocity and headway without using large acceleration/deceleration, we minimize a cost function containing its headway and velocity fluctuations and its acceleration. The solution will give the gains for the CCC vehicle with respect to the current and delayed headways and velocities of the vehicles ahead.

Let us define

$$x_i = \begin{bmatrix} N^*\tilde{h}_i - \tilde{v}_i \\ \tilde{v}_{i+1} - \tilde{v}_i \end{bmatrix}, \quad \phi_n = \begin{bmatrix} 0 \\ \dot{\tilde{v}}_{n+1} \end{bmatrix}. \tag{13}$$

Then we construct the vectors

$$X = \begin{bmatrix} x_1 \\ \vdots \\ x_n \end{bmatrix}, \quad \phi = \begin{bmatrix} 0 \\ \vdots \\ 0 \\ \phi_n \end{bmatrix}, \tag{14}$$

and rewrite (10,12) as

$$\dot{X}(t) = \mathbf{A}X(t) + \mathbf{B}X(t-\tau) + \mathbf{D}u(t) + \phi(t)\,. \tag{15}$$

The coefficient matrices are given by

$$\mathbf{A} = \mathbf{I}_n \otimes \mathbf{A}_1, \quad \mathbf{B} = \begin{bmatrix} \mathbf{0} & \mathbf{B}_2 & & \\ \mathbf{B}_1 & \mathbf{B}_2 & & \\ & \ddots & \ddots & \\ & & \mathbf{B}_1 & \mathbf{B}_2 \\ & & & \mathbf{B}_1 \end{bmatrix}, \quad \mathbf{D} = \begin{bmatrix} \mathbf{D}_1 \\ \mathbf{0} \\ \vdots \\ \mathbf{0} \\ \mathbf{0} \end{bmatrix}, \tag{16}$$

where $\otimes$ denotes the Kronecker product and the blocks are defined by

$$\mathbf{A}_1 = \begin{bmatrix} 0 & N^* \\ 0 & 0 \end{bmatrix}, \ \mathbf{B}_1 = -\begin{bmatrix} \alpha & \beta \\ \alpha & \beta \end{bmatrix}, \ \mathbf{B}_2 = \begin{bmatrix} 0 & 0 \\ \alpha & \beta \end{bmatrix}, \ \mathbf{D}_1 = \begin{bmatrix} -1 \\ -1 \end{bmatrix}. \tag{17}$$

Note that $\mathbf{B}$ is upper block-triangular because vehicles only react to the motion of vehicles ahead. This topological structure of connectivity will allow us to greatly simplify the solution of the LQR problem.

We assume that the non-CCC vehicles are plant stable, i.e., they are able to maintain the uniform flow (6) when the vehicles ahead travel with constant speed v^*. Then the connected vehicle system (15,16) is stabilizable, that is, uncontrollable part of the system is stable.

We define the multi-objective cost function based on the CCC vehicle's acceleration and deviations from the uniform flow as

$$\begin{aligned} J_{t_\mathrm{f}}(u, X) &= \int_0^{t_\mathrm{f}} \Big(\dot{\tilde{v}}_1^2 + \gamma_1 \big(N^*\tilde{h}_1 - \tilde{v}_1\big)^2 + \gamma_2 \big(\tilde{v}_2 - \tilde{v}_1\big)^2 \Big) \mathrm{d}t \\ &= \int_0^{t_\mathrm{f}} \big(u^2 + X^\mathrm{T} \mathbf{\Gamma} X \big) \mathrm{d}t\,, \end{aligned} \tag{18}$$

where $\gamma_1 > 0$, $\gamma_2 > 0$ and

$$\mathbf{\Gamma} = \mathrm{diag}[\gamma_1, \gamma_2, 0, \ldots, 0] \in \mathbb{R}^{2n \times 2n}. \tag{19}$$

In (18) the first term is related with the fuel economy of the CCC vehicle, and the latter two terms account for the active safety and traffic efficiency. While more complicated cost functions can be used to consider more accurate powertrain dynamics [14], [37], the quadratic form of (18) will provide us with valuable insight about the upper-level control of connected vehicle systems.

B. General Solution of the LQ Problem

In this section we lay out the general solution to the LQ problem in a time-delayed system with disturbance (15,18). We will show that the disturbance has limited influence on the structure of the optimal controller. Thus, we design the optimal controller under zero disturbance. This setting allows us to

exploit the uni-directional information flow to alleviate the high computational cost for optimal connected vehicle design. Readers not interested in the technical details may proceed to Section III-D.

We define the augmented state $Y(t) = [X^{\mathrm{T}}(t) \;\; 1]^{\mathrm{T}}$ to place the disturbance term $\phi(t)$ in (15) into a time-variant coefficient matrix. This yields

$$\dot{Y}(t) = \tilde{\mathbf{A}}(t)Y(t) + \tilde{\mathbf{B}}Y(t-\tau) + \tilde{\mathbf{D}}u(t)\,, \tag{20}$$

where

$$\tilde{\mathbf{A}}(t) = \begin{bmatrix} \mathbf{A} & \phi(t) \\ 0 & 0 \end{bmatrix}, \quad \tilde{\mathbf{B}} = \begin{bmatrix} \mathbf{B} & 0 \\ 0 & 0 \end{bmatrix}, \quad \tilde{\mathbf{D}} = \begin{bmatrix} \mathbf{D} \\ 0 \end{bmatrix}. \tag{21}$$

The cost function (18) can be rewritten accordingly

$$J_{t_{\mathrm{f}}}(u, Y) = \int_0^{t_{\mathrm{f}}} \left(u^2 + Y^{\mathrm{T}} \tilde{\mathbf{\Gamma}} Y \right) \mathrm{d}t\,, \tag{22}$$

where $\tilde{\mathbf{\Gamma}} = \begin{bmatrix} \Gamma & 0 \\ 0 & 0 \end{bmatrix}$.

The optimal control for (20,22) is given by

$$u(t) = -\tilde{\mathbf{D}}^{\mathrm{T}} \left(\mathbf{P}(t)Y(t) + \int_{-\tau}^{0} \mathbf{Q}(t,\theta)Y(t+\theta)\mathrm{d}\theta \right), \tag{23}$$

see [38]. The matrices $\mathbf{P}(t)$ and $\mathbf{Q}(t,\theta)$ are obtained by solving the Riccati-type partial differential equation (PDE)

$$\begin{aligned} -\dot{\mathbf{P}}(t) &= \tilde{\mathbf{A}}^{\mathrm{T}}\mathbf{P}(t) + \mathbf{P}(t)\tilde{\mathbf{A}} - \mathbf{P}(t)\tilde{\mathbf{D}}\tilde{\mathbf{D}}^{\mathrm{T}}\mathbf{P}(t) \\ &\quad + \mathbf{Q}(t,0) + \mathbf{Q}^{\mathrm{T}}(t,0) + \tilde{\mathbf{\Gamma}}\,, \\ (\partial_\theta - \partial_t)\mathbf{Q}(t,\theta) &= \left(\tilde{\mathbf{A}}^{\mathrm{T}} - \mathbf{P}\tilde{\mathbf{D}}\tilde{\mathbf{D}}^{\mathrm{T}}\right)\mathbf{Q}(t,\theta) + \mathbf{R}(t,0,\theta)\,, \\ (\partial_\xi + \partial_\theta - \partial_t)\mathbf{R}(t,\xi,\theta) &= -\mathbf{Q}^{\mathrm{T}}(t,\xi)\tilde{\mathbf{D}}\tilde{\mathbf{D}}^{\mathrm{T}}\mathbf{Q}(t,\theta)\,, \end{aligned} \tag{24}$$

with boundary conditions

$$\begin{aligned} &\mathbf{P}(t_{\mathrm{f}}) = \mathbf{0}\,, \\ &\mathbf{Q}(t_{\mathrm{f}},\theta) = \mathbf{0}\,, \qquad \mathbf{Q}(t,-\tau) = \mathbf{P}^{\mathrm{T}}\tilde{\mathbf{B}}\,, \\ &\mathbf{R}(t_{\mathrm{f}},\xi,\theta) = \mathbf{0}\,, \quad \mathbf{R}(t,-\tau,\theta) = \tilde{\mathbf{B}}^{\mathrm{T}}\mathbf{Q}(t,\theta)\,, \end{aligned} \tag{25}$$

where $\mathbf{P}(t)$ is symmetric and $\mathbf{R}^{\mathrm{T}}(t,\xi,\theta) = \mathbf{R}(t,\theta,\xi)$. Given the structure of coefficient matrices (21), the matrices $\mathbf{P}(t)$, $\mathbf{Q}(t,\theta)$ and $\mathbf{R}(t,\xi,\theta)$ can be constructed as

$$\mathbf{P} = \begin{bmatrix} \mathbf{P}_1 & \mathbf{P}_2 \\ \mathbf{P}_3 & \mathbf{P}_4 \end{bmatrix}, \; \mathbf{Q} = \begin{bmatrix} \mathbf{Q}_1 & \mathbf{Q}_2 \\ \mathbf{Q}_3 & \mathbf{Q}_4 \end{bmatrix}, \; \mathbf{R} = \begin{bmatrix} \mathbf{R}_1 & \mathbf{R}_2 \\ \mathbf{R}_3 & \mathbf{R}_4 \end{bmatrix}, \tag{26}$$

where $\mathbf{P}_1, \mathbf{Q}_1, \mathbf{R}_1 \in \mathbb{R}^{2n\times 2n}$, $\mathbf{P}_2, \mathbf{Q}_2, \mathbf{R}_2 \in \mathbb{R}^{2n\times 1}$, $\mathbf{P}_3, \mathbf{Q}_3, \mathbf{R}_3 \in \mathbb{R}^{1\times 2n}$, and $\mathbf{P}_4, \mathbf{Q}_4, \mathbf{R}_4$ are scalars. since $\mathbf{P}(t)$ is symmetric we have $\mathbf{P}_1(t) = \mathbf{P}_1^{\mathrm{T}}(t)$ and $\mathbf{P}_2(t) = \mathbf{P}_3^{\mathrm{T}}(t)$. Moreover, $\mathbf{R}(t,\xi,\theta) = \mathbf{R}^{\mathrm{T}}(t,\theta,\xi)$ yields $\mathbf{R}_1(t,\xi,\theta) = \mathbf{R}_1^{\mathrm{T}}(t,\theta,\xi)$ and $\mathbf{R}_2(t,\xi,\theta) = \mathbf{R}_3^{\mathrm{T}}(t,\theta,\xi)$. Thus, the optimal controller (23) becomes

$$\begin{aligned} u(t) = -\mathbf{D}^{\mathrm{T}} \Bigg(&\mathbf{P}_1(t)X(t) + \int_{-\tau}^{0} \mathbf{Q}_1(t,\theta)X(t+\theta)\mathrm{d}\theta \\ &+ \mathbf{P}_2(t) + \int_{-\tau}^{0} \mathbf{Q}_2(t,\theta)\mathrm{d}\theta \Bigg). \end{aligned} \tag{27}$$

By substituting (26) into (24,25) we find that state-feedback-control gain matrices $\mathbf{P}_1, \mathbf{Q}_1$ in the optimal controller (27) are not influenced by the disturbance $\phi(t)$; see (65,67,69,71) in Appendix A. On the other hand, when including the disturbance in the optimization, (27) cannot be implemented in real time since $\phi(t)$ is not known a priori; cf. $\tilde{\mathbf{A}}(t)$ in (21,24,26). Therefore we first ignore the disturbance $\phi(t)$, but later in Section IV we ensure that this zero-disturbance design can reject disturbances satisfyingly. Thus, we consider

$$\mathbf{P}_2(t) \equiv \mathbf{0}\,, \qquad \mathbf{Q}_2(t,\theta) \equiv \mathbf{0}\,, \tag{28}$$

which allows us to design the CCC controller analytically without impairing the stability of the multi-vehicle system.

Since $\mathbf{P}_1(t), \mathbf{Q}_1(t,\theta), \mathbf{R}_1(t,\xi,\theta)$ are given by (65), which is an initial value problem in backward time, we consider the steady-state solution

$$\mathbf{P}_1(t) \equiv \mathbf{P}_1, \quad \mathbf{Q}_1(t,\theta) \equiv \mathbf{Q}_1(\theta), \quad \mathbf{R}_1(t,\xi,\theta) \equiv \mathbf{R}_1(\xi,\theta), \tag{29}$$

which is equivalent to setting time horizon $t_{\mathrm{f}} \to \infty$ in the cost function (18); see [39].

Substituting (28,29) into (27) leads to the simplified controller

$$u(t) = -\mathbf{D}^{\mathrm{T}} \left(\mathbf{P}_1 X(t) + \int_{-\tau}^{0} \mathbf{Q}_1(\theta)X(t+\theta)\mathrm{d}\theta \right), \tag{30}$$

where the matrices $\mathbf{P}_1$, $\mathbf{Q}_1(\theta)$ are given by

$$\begin{aligned} &\mathbf{A}^{\mathrm{T}}\mathbf{P}_1 + \mathbf{P}_1\mathbf{A} - \mathbf{P}_1\mathbf{D}\mathbf{D}^{\mathrm{T}}\mathbf{P}_1 + \mathbf{Q}_1(0) + \mathbf{Q}_1^{\mathrm{T}}(0) + \mathbf{\Gamma} = \mathbf{0}\,, \\ &\partial_\theta \mathbf{Q}_1(\theta) = \left(\mathbf{A}^{\mathrm{T}} - \mathbf{P}_1\mathbf{D}\mathbf{D}^{\mathrm{T}}\right)\mathbf{Q}_1(\theta) + \mathbf{R}_1(0,\theta)\,, \\ &(\partial_\xi + \partial_\theta)\mathbf{R}_1(\xi,\theta) = -\mathbf{Q}_1^{\mathrm{T}}(\xi)\mathbf{D}\mathbf{D}^{\mathrm{T}}\mathbf{Q}_1(\theta)\,, \end{aligned} \tag{31}$$

with boundary conditions

$$\mathbf{Q}_1(-\tau) = \mathbf{P}_1\mathbf{B}\,, \qquad \mathbf{R}_1(-\tau,\theta) = \mathbf{B}^{\mathrm{T}}\mathbf{Q}_1(\theta)\,, \tag{32}$$

which can be attained by setting $t_{\mathrm{f}} \to \infty$ in (65,66).

C. Decomposition of the Solution

In this section, we exploit the uni-directional information flow and obtain the analytical solution to the delayed LQ problem (15,18) with zero disturbance ($\phi(t) \equiv 0$) and infinite time horizon ($t_{\mathrm{f}} = \infty$), i.e., we solve the PDE (31,32) analytically to obtain the controller (30).

While a numerical scheme for (31,32) is given in [39] to obtain $\mathbf{P}_1$, $\mathbf{Q}_1(\theta)$ in (30), no closed-form solution exists with general $\mathbf{A}, \mathbf{B}, \mathbf{D}$ matrices. However, here only the first two rows of $\mathbf{P}_1, \mathbf{Q}_1(\theta)$ are used by the controller (30), since $\mathbf{D}$ is zero except its first two elements, cf. (16,17). Thus we only need to obtain an analytical solution for the relevant parts in $\mathbf{P}_1$, $\mathbf{Q}_1(\theta)$, which is made possible by taking advantage of the upper-triangular block structure of $\mathbf{A}$ and $\mathbf{B}$.

We introduce the notation

$$\mathbf{P}_1 = \begin{bmatrix} \mathbf{P}_{11} & \cdots & \mathbf{P}_{1n} \\ \vdots & \ddots & \vdots \\ \mathbf{P}_{n1} & \cdots & \mathbf{P}_{nn} \end{bmatrix}, \quad \mathbf{Q}_1(\theta) = \begin{bmatrix} \mathbf{Q}_{11}(\theta) & \cdots & \mathbf{Q}_{1n}(\theta) \\ \vdots & \ddots & \vdots \\ \mathbf{Q}_{n1}(\theta) & \cdots & \mathbf{Q}_{nn}(\theta) \end{bmatrix}, \tag{33}$$

where $\mathbf{P}_{ij}, \mathbf{Q}_{ij}(\theta) \in \mathbb{R}^{2\times 2}$ for $i, j = 1, \ldots, n$, and rewrite (30) as

$$u(t) = -\mathbf{D}_1^{\mathrm{T}} \sum_{i=1}^{n} \left(\mathbf{P}_{1i}x_i(t) + \int_{-\tau}^{0} \mathbf{Q}_{1i}(\theta)x_i(t+\theta)\mathrm{d}\theta \right), \tag{34}$$

where $x_i(t)$ is given in (13). This shows that we only need to derive $\mathbf{P}_{1i}, \mathbf{Q}_{1i}(\theta)$ for $i = 1, \dots, n$ to construct the controller. Substituting (33) into (31,32), we obtain equations for each block $\mathbf{P}_{ij}, \mathbf{Q}_{ij}(\theta), \mathbf{R}_{ij}(\xi, \theta)$, $i, j = 1, \dots, n$, which can be solved recursively. Specifically, $\mathbf{P}_{11}$ and $\mathbf{Q}_{11}(\theta)$ are given by

$$\begin{aligned} &\hat{\mathbf{A}}_1\mathbf{P}_{11} + \mathbf{P}_{11}\mathbf{A}_1 + \mathbf{Q}_{11}(0) + \mathbf{Q}_{11}^{\mathrm{T}}(0) + \mathrm{diag}[\gamma_1, \gamma_2] = \mathbf{0}\,, \\ &\partial_\theta \mathbf{Q}_{11}(\theta) = \hat{\mathbf{A}}_1\mathbf{Q}_{11}(\theta) + \mathbf{R}_{11}(0, \theta)\,, \\ &(\partial_\xi + \partial_\theta)\mathbf{R}_{11}(\xi, \theta) = -\mathbf{Q}_{11}^{\mathrm{T}}(\xi)\mathbf{D}\mathbf{D}^{\mathrm{T}}\mathbf{Q}_{11}(\theta)\,, \end{aligned} \tag{35}$$

with boundary conditions

$$\mathbf{Q}_{11}(-\tau) = \mathbf{0}\,, \qquad \mathbf{R}_{11}(-\tau, \theta) = \mathbf{0}\,, \tag{36}$$

where

$$\hat{\mathbf{A}}_1 = \mathbf{A}_1^{\mathrm{T}} - \mathbf{P}_{11}\mathbf{D}_1\mathbf{D}_1^{\mathrm{T}}\,. \tag{37}$$

The solution of (35,36) is given by

$$\mathbf{P}_{11} = \begin{bmatrix} p_{11} & p_{12} \\ p_{12} & p_{22} \end{bmatrix}, \quad \mathbf{Q}_{11}(\theta) \equiv \mathbf{0}, \quad \mathbf{R}_{11}(\xi, \theta) \equiv \mathbf{0}\,, \tag{38}$$

where

$$\begin{aligned} p_{11} &= \frac{-\gamma_1 + \sqrt{\gamma_1}\sqrt{\gamma_1 + \gamma_2 + 2N^*\sqrt{\gamma_1}}}{N^*}\,, \\ p_{12} &= \sqrt{\gamma_1} - p_{11}\,, \\ p_{22} &= -2\sqrt{\gamma_1} + \sqrt{\gamma_1 + \gamma_2 + 2N^*\sqrt{\gamma_1}} + p_{11}\,, \end{aligned} \tag{39}$$

which is the only solution satisfying the condition $\mathbf{P}_{11} > \mathbf{0}$. Notice that the matrix $\mathbf{P}_{11}$ only depends on the weights γ_1, γ_2 and the CCC vehicle's range policy N^* (cf. (3)).

Then, to obtain $\mathbf{P}_{1i}, \mathbf{Q}_{1i}(\theta), \mathbf{Q}_{i1}(\theta)$ for $i = 2, \dots, n$, we need to solve

$$\begin{aligned} &\hat{\mathbf{A}}_1\mathbf{P}_{1i} + \mathbf{P}_{1i}\mathbf{A}_1 + \mathbf{Q}_{1i}(0) + \mathbf{Q}_{i1}^{\mathrm{T}}(0) = \mathbf{0}\,, \\ &\partial_\theta \mathbf{Q}_{1i}(\theta) = \hat{\mathbf{A}}_1\mathbf{Q}_{1i}(\theta) + \mathbf{R}_{1i}(0, \theta)\,, \\ &\partial_\theta \mathbf{Q}_{i1}(\theta) = \mathbf{A}_1^{\mathrm{T}}\mathbf{Q}_{i1}(\theta) - \mathbf{P}_{1i}^{\mathrm{T}}\mathbf{D}_1\mathbf{D}_1^{\mathrm{T}}\mathbf{Q}_{11}(\theta) + \mathbf{R}_{1i}^{\mathrm{T}}(\theta, 0)\,, \\ &(\partial_\xi + \partial_\theta)\mathbf{R}_{1i}(\xi, \theta) = -\mathbf{Q}_{11}^{\mathrm{T}}(\xi)\mathbf{D}_1\mathbf{D}_1^{\mathrm{T}}\mathbf{Q}_{1i}(\theta)\,, \end{aligned} \tag{40}$$

with boundary conditions

$$\begin{aligned} &\mathbf{Q}_{1i}(-\tau) = \mathbf{P}_{1i}\mathbf{B}_1 + \mathbf{P}_{1(i-1)}\mathbf{B}_2\,, \\ &\mathbf{Q}_{i1}(-\tau) = \mathbf{0}\,, \\ &\mathbf{R}_{1i}(\theta, -\tau) = \mathbf{Q}_{i1}^{\mathrm{T}}(\theta)\mathbf{B}_1 + \mathbf{Q}_{(i-1)1}^{\mathrm{T}}(\theta)\mathbf{B}_2\,, \\ &\mathbf{R}_{1i}(-\tau, \theta) = \mathbf{0}\,. \end{aligned} \tag{41}$$

Now (40,41) give the solution

$$\mathbf{Q}_{i1}(\theta) \equiv \mathbf{0}, \quad \mathbf{R}_{1i}(\xi, \theta) \equiv \mathbf{0}\,, \tag{42}$$

while the equations for $\mathbf{Q}_{1i}(\theta)$ simplify to

$$\begin{aligned} \partial_\theta \mathbf{Q}_{1i}(\theta) &= \hat{\mathbf{A}}_1\mathbf{Q}_{1i}(\theta), \\ \mathbf{Q}_{1i}(-\tau) &= \mathbf{P}_{1i}\mathbf{B}_1 + \mathbf{P}_{1(i-1)}\mathbf{B}_2\,, \end{aligned} \tag{43}$$

yielding the solution

$$\mathbf{Q}_{1i}(\theta) = \mathrm{e}^{\hat{\mathbf{A}}_1(\theta+\tau)}(\mathbf{P}_{1i}\mathbf{B}_1 + \mathbf{P}_{1(i-1)}\mathbf{B}_2)\,, \tag{44}$$

for $i = 2, \dots, n$. Thus, the equation for $\mathbf{P}_{1i}$ becomes

$$\hat{\mathbf{A}}_1\mathbf{P}_{1i} + \mathbf{P}_{1i}\mathbf{A}_1 + \mathrm{e}^{\tau\hat{\mathbf{A}}_1}(\mathbf{P}_{1i}\mathbf{B}_1 + \mathbf{P}_{1(i-1)}\mathbf{B}_2) = \mathbf{0}\,, \tag{45}$$

yielding the solution

$$\mathrm{vec}(\mathbf{P}_{1i}) = \mathbf{M}^{i-1}\mathrm{vec}(\mathbf{P}_{11})\,, \tag{46}$$

for $i = 2, \dots, n$. Here $\mathrm{vec}(\cdot)$ gives a column vector by stacking the columns of the matrix on the top of each other, and $\mathbf{M} \in \mathbb{R}^{4\times 4}$ is given by

$$\mathbf{M} = -\big(\mathbf{I} \otimes \hat{\mathbf{A}}_1 + \mathbf{A}_1^{\mathrm{T}} \otimes \mathbf{I} + \mathbf{B}_1^{\mathrm{T}} \otimes \mathrm{e}^{\tau\hat{\mathbf{A}}_1}\big)^{-1}\big(\mathbf{B}_2^{\mathrm{T}} \otimes \mathrm{e}^{\tau\hat{\mathbf{A}}_1}\big)\,. \tag{47}$$

Consequently, $\mathbf{P}_{1i}$ and $\mathbf{Q}_{1i}(\theta)$ are obtained recursively using (38,44,46,47). The recursive rules (44,46) indicate that the feedback gains for signals coming from the j^{th} vehicle only depend on the dynamics of vehicles 2 to j and do not depend on the dynamics of vehicles in front of the j^{th} vehicle. On the other hand, since $\hat{\mathbf{A}}_1$ only depends on $\mathbf{P}_{11}$ (cf. (37,38,39)), the exponential term $\mathrm{e}^{\hat{\mathbf{A}}_1(\theta+\tau)}$ shared by every $\mathbf{Q}_{1i}(\theta)$ is independent from the dynamics of preceding vehicles but changes with the CCC vehicle's range policy N^* and the optimization weights γ_1, γ_2.

D. Constructing the CCC Controller

In (34) we move $\mathbf{D}_1$ (cf. (16)) into the integral and define

$$\begin{aligned} \begin{bmatrix} \alpha_{1i} & \beta_{1i} \end{bmatrix} &= \begin{bmatrix} 1 & 1 \end{bmatrix}\mathbf{P}_{1i}, \\ \begin{bmatrix} f_i(\theta) & g_i(\theta) \end{bmatrix} &= \begin{bmatrix} 1 & 1 \end{bmatrix}\mathbf{Q}_{1i}(\theta)\,. \end{aligned} \tag{48}$$

Based on definitions (13,48), the optimal controller (34) for the CCC vehicle is given by

$$\begin{aligned} u(t) = &\sum_{i=1}^{n}\Big(\alpha_{1i}\big(N^*\tilde{h}_i(t) - \tilde{v}_i(t)\big) + \beta_{1i}\big(\tilde{v}_{i+1}(t) - \tilde{v}_i(t)\big)\Big) \\ &+ \sum_{i=1}^{n}\int_{-\tau}^{0} f_i(\theta)\big(N^*\tilde{h}_i(t+\theta) - \tilde{v}_i(t+\theta)\big)\mathrm{d}\theta \\ &+ \sum_{i=1}^{n}\int_{-\tau}^{0} g_i(\theta)\big(\tilde{v}_{i+1}(t+\theta) - \tilde{v}_i(t+\theta)\big)\mathrm{d}\theta\,, \end{aligned} \tag{49}$$

where the distribution kernels take the form

$$\begin{aligned} f_i(\theta) &= \big(a_{i0} + a_{i1}(\theta+\tau)\big)\mathrm{e}^{\lambda_1(\theta+\tau)} + a_{i2}\mathrm{e}^{\lambda_2(\theta+\tau)}\,, \\ g_i(\theta) &= \big(b_{i0} + b_{i1}(\theta+\tau)\big)\mathrm{e}^{\lambda_1(\theta+\tau)} + b_{i2}\mathrm{e}^{\lambda_2(\theta+\tau)}\,, \end{aligned} \tag{50}$$

for $i = 1, \dots, n$, $\theta \in [-\tau, 0]$, where λ_1, λ_2 are the eigenvalues of $\hat{\mathbf{A}}_1$, and the expressions for $\lambda_1, \lambda_2, a_{i0}, a_{i1}, a_{i2}$, and b_{i0}, b_{i1}, b_{i2} are given in Appendix B.

From (38,39,48) we obtain that

$$\alpha_{11} = \sqrt{\gamma_1}, \quad \beta_{11} = -\sqrt{\gamma_1} + \sqrt{\gamma_1 + \gamma_2 + 2N^*\sqrt{\gamma_1}}\,, \tag{51}$$

i.e., the gains on CCC vehicle's own headway and velocity do not depend on the dynamics of human-driven vehicles. Since $\mathbf{Q}_{11}(\theta) \equiv \mathbf{0}$, (48) yields

$$f_1(\theta) \equiv 0, \quad g_1(\theta) \equiv 0\,, \tag{52}$$

i.e., the CCC vehicle does not have delayed feedback terms on its own headway and velocity. The rest of the gains α_{1i}, β_{1i} and the distribution kernels $f_i(\theta)$, $g_i(\theta)$ for $i = 2, \dots, n$ in (48) can be obtained using (44,46,47).

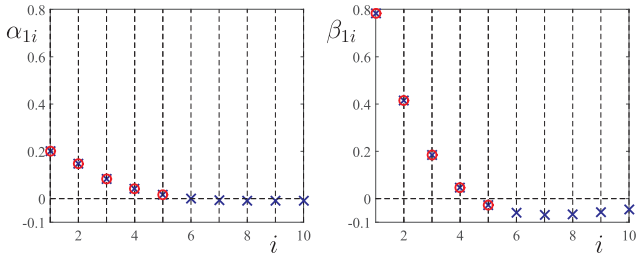

Fig. 4. The optimized feedback gains $\alpha_{1i}, \beta_{1i}, i = 1, \ldots, n$ of the CCC vehicle in a string of $(n+1)$ vehicles for $n = 5$ (red circles) and for $n = 10$ (blue crosses). The human parameters are $\alpha = 0.6$ [1/s], $\beta = 0.9$ [1/s], $\tau = 0.4$ [s]. The design parameters are $\gamma_1 = 0.04\,[1/\mathrm{s}^2]$, $\gamma_2 = 0.30\,[1/\mathrm{s}^2]$.

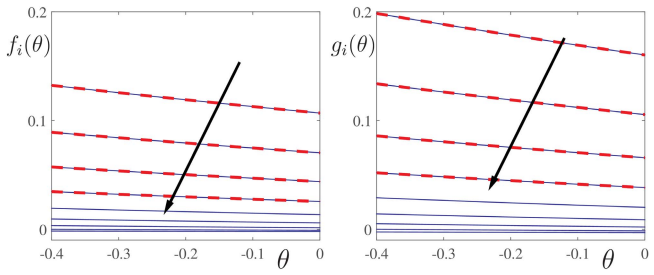

Fig. 5. The optimized distribution kernels $f_i(\theta), g_i(\theta)$ for $i = 2, \ldots, n$ of the CCC vehicle for a $(n+1)$-car system with the same parameter as in Fig. 4. The red dashed curves correspond to $n = 5$, and the blue solid curves correspond to $n = 10$. The black arrows show the direction of increasing vehicle index i.

In Appendix C we show that the eigenvalues of $\mathbf{M}$ (cf. (47)) are inside the unit circle for realistic values of weights γ_1, γ_2, human gains α, β, and driver reaction time τ. Thus (46) is a contracting map. Since α_{1i}, β_{1i} are given in (48) as linear combinations of the components of $\mathbf{P}_{1i}$, they converge to zero as i increases.

Fig. 4 shows the corresponding exponential decay of α_{1i} and β_{1i} in a $(5+1)$ vehicle chain (red circles) and a $(10+1)$ vehicle chain (blue crosses) using the parameter values $\gamma_1 = 0.04\,[1/\mathrm{s}^2]$, $\gamma_2 = 0.30\,[1/\mathrm{s}]$, $\alpha = 0.6\,[1/\mathrm{s}]$, $\beta = 0.9\,[1/\mathrm{s}]$ and $\tau = 0.4\,[\mathrm{s}]$. In this case, $\mathbf{M}$ has two zero eigenvalues and two non-zero eigenvalues $0.69 \pm 0.15i$. The exact match between the red circles and the blue crosses for vehicles 2 to 5 demonstrates that the existing optimized gains do not change when adding feedback terms on vehicles farther away. This corresponds to the fact that the gains α_{11}, β_{11} are not influenced by the connectivity structure (cf. (38,39,48)), and that α_{1i}, β_{1i} are calculated recursively using (46). For the parameters considered above, we have the gains $\alpha_{11} \approx 0.20\,[1/\mathrm{s}]$, $\beta_{11} \approx 0.78\,[1/\mathrm{s}]$.

In Fig. 5 we plot the distribution kernels $f_i(\theta), g_i(\theta)$ for $i = 2, \ldots, n$ using the same parameters as in Fig. 4. The dashed red curves correspond to $n = 5$ and the blue solid curves correspond to $n = 10$. In both cases, the magnitude of $f_i(\theta)$ and $g_i(\theta)$ decreases with i. Indeed, for vehicles $i = 2, \ldots, 5$, the distribution kernels $f_i(\theta)$ and $g_i(\theta)$ are the same in both the $(5+1)$-car and the $(10+1)$-car systems.

Considering the similar feedback structure of the CCC controller (49) as in the conventional driving model (2), and the decay of feedback gains and distribution kernels shown in Fig. 4 and Fig. 5, we conclude that the proposed CCC controller will degrade gracefully under imperfect communication. More specifically, a CCC vehicle may experience severe packet drops from vehicles ahead, depending on the involved V2V communication devices, the physical distance between vehicles and the road environment [40]. When the communication channel with vehicle $i+1$ significantly deteriorates, we may set the feedback gains and distribution kernels corresponding to vehicle $i+1$ and vehicles farther ahead as zero, and only use motion signals up to vehicles i. Since motion signals from farther downstream vehicles are assigned with smaller gains, the switch to fewer signals will not induce a significant jump in control commands. Most importantly, since the gains for signals coming from vehicles 1–i do not depend on those from vehicles $i+1$ and beyond, the reduced CCC controller still remains optimal.

We note that the proposed CCC controller generates $2n$ feedback gains and distribution kernels with only 2 design parameters, while being robust against heterogeneity and connectivity structure changes among preceding vehicles, as discussed in detail in Appendix D. While our design relies on car-following models in the form of (1) for the human-driven vehicles ahead, one may use other driver models (see [23]) to design similar controllers.

IV. Stability Analysis of Optimized Connected Vehicle Systems

In this section, we analyze the linear stability of uniform traffic flow using the optimized controller for the CCC vehicle at the tail, to make sure that the arising connected vehicle system is able to maintain uniform traffic flow. Here we take into account the communication delay due to intermittency and packet loss in wireless communication. We analyze the plant stability and head-to-tail string stability and visualize the corresponding stability areas using stability charts.

The intermittency in V2V communication with digital controllers results in an average communication delay of 0.15 [s]; see [16]. However, packet losses may lead to significant increase of the delay. While the delay changes stochastically [20], here we approximate it with its average and study the dynamics while viewing the delay as a parameter. Then the linear dynamics (10,12) becomes

$$\begin{aligned}
\dot{\tilde{h}}_1(t) &= \tilde{v}_2(t) - \tilde{v}_1(t)\,,\\
\dot{\tilde{v}}_1(t) &= u(t-\sigma)\,,\\
\dot{\tilde{h}}_i(t) &= \tilde{v}_{i+1}(t) - \tilde{v}_i(t)\,,\\
\dot{\tilde{v}}_i(t) &= \alpha\big(N^*\tilde{h}_i(t-\tau) - \tilde{v}_i(t-\tau)\big)\\
&\quad + \beta\big(\tilde{v}_{i+1}(t-\tau) - \tilde{v}_i(t-\tau)\big),
\end{aligned} \tag{53}$$

for $i = 2, \ldots, n$, where $u(t)$ is given by (49) and σ denotes the communication delay.

The plant stability of a CCC vehicle is given as follows: suppose that the vehicles whose signals are used by the CCC vehicle are driven at the same constant velocity, that is, $v_i(t) \equiv v^*$, $i = 2, \ldots, n+1$, then the velocity of the CCC vehicle approaches this constant velocity, i.e., $\lim_{t\to\infty} v_1(t) = v^*$.

The plant stability of non-CCC vehicles is defined similarly: when the preceding vehicle is driven at constant velocity, the non-CCC vehicle should converge to the same velocity. In this paper we only consider plant stable non-CCC vehicles.

String stability characterizes the attenuation of velocity fluctuations as they propagate upstream [36]. For non-CCC vehicles it is required that the vehicle attenuates the velocity fluctuations arising from the preceding vehicle. For a CCC vehicle, one may compare its velocity fluctuations with any preceding vehicle whose signals is used by the CCC vehicle. The influence of a CCC vehicle on the traffic flow is evaluated the best by comparing its velocity fluctuations to that of the furthest vehicle ahead whose signal is received by the CCC vehicle (called the head vehicle). Thus, we define the head-to-tail string stability, which requires velocity fluctuations to be suppressed from the head vehicle to the tail. Since no control is placed upon the non-CCC vehicles, it is reasonable to allow amplification of velocity fluctuations among non-CCC vehicles. Still, the CCC vehicles may ensure head-to-tail string stability as demonstrated below.

While in the previous section the controller was designed for the zero disturbance case, here we consider the velocity perturbation $\tilde{v}_{n+1}$ of the head vehicle as the input and the velocity perturbation $\tilde{v}_1$ of the tail vehicle as the output in (53). Since perturbations of velocity can be represented using Fourier components and superposition holds for linear systems, the head-to-tail string stability can be ensured by attenuating sinusoidal signals for all excitation frequencies. Thus, we consider the periodic excitation $\tilde{v}_{n+1}(t) = v_{n+1}^{\text{amp}} \sin(\omega t)$ with frequency ω and amplitude v_{n+1}^{amp}. Then the steady state response of (53) with control (49) is $\tilde{v}_{1,\text{ss}}(t) = v_1^{\text{amp}} \sin(\omega t + \psi)$. In order to ensure head-to-tail string stability, we need the amplitude ratio $v_1^{\text{amp}}/v_{n+1}^{\text{amp}} < 1$ for all excitation frequencies $\omega > 0$, which can be obtained through transfer functions.

In particular, taking the Laplace transform of (53) with zero initial conditions and eliminating the velocities and headways of vehicles $i = 2, \ldots, n$, we obtain the head-to-tail transfer function

$$H(s) = \frac{\tilde{V}_1(s)}{\tilde{V}_{n+1}(s)} = \frac{\sum_{i=2}^{n} \big(F_{i-1}(s) - G_i(s)\big) \cdot \big(H_0(s)\big)^{n-i+1} + F_n(s)}{s^2 \mathrm{e}^{\sigma s} + G_1(s)} . \tag{54}$$

Here $\tilde{V}_1(s)$ and $\tilde{V}_{n+1}(s)$ denote the Laplace transform of $\tilde{v}_1(t)$ and $\tilde{v}_{n+1}(t)$, respectively, and

$$\begin{aligned} H_0(s) &= \frac{F_0(s)}{G_0(s)} = \frac{\beta s + \alpha N^*}{s^2 \mathrm{e}^{\tau s} + (\alpha + \beta) s + \alpha N^*} , \\ F_i(s) &= \alpha_{1i} N^* + \beta_{1i} s + (a_{i1} N^* + b_{i1} s) h_1(s) \\ &\quad + (a_{i0} N^* + b_{i0} s) h_0(s) + (a_{i2} N^* + b_{i2} s) h_2(s) , \\ G_i(s) &= F_i(s) + \alpha_{1i} s + s\big(a_{i0} h_0(s) + a_{i1} h_1(s) + a_{i2} h_2(s)\big) , \end{aligned} \tag{55}$$

where $a_{i0}, a_{i1}, a_{i2}, b_{i0}, b_{i1}, b_{i2}$ are given in Appendix B for $i = 1, \ldots, n$ and

$$\begin{aligned} h_0(s) &= \frac{\mathrm{e}^{\tau \lambda_1} - \mathrm{e}^{-\tau s}}{s + \lambda_1} , \\ h_1(s) &= \frac{\tau \mathrm{e}^{-\tau s}}{s + \lambda_1} - \frac{\mathrm{e}^{\tau \lambda_1} - \mathrm{e}^{-\tau s}}{(s + \lambda_1)^2} , \\ h_2(s) &= \frac{\mathrm{e}^{\tau \lambda_2} - \mathrm{e}^{-\tau s}}{s + \lambda_2} . \end{aligned} \tag{56}$$

Here $H_0(s)$ represents the transfer function between a non-CCC vehicle and its predecessor. Indeed, the amplitude ratio for frequency ω is given by $v_1^{\text{amp}}/v_{n+1}^{\text{amp}} = |H(\mathrm{i}\omega)|$, that is, the head-to-tail string stability is ensured when $|H(\mathrm{i}\omega)| < 1$ for all $\omega > 0$.

A. Plant Stability

The plant stability for the linearized connected vehicle system (49,53) requires that all its characteristic roots have negative real parts, i.e., the solutions of the characteristic equation

$$G_0^{n-1}(s)\big(s^2 \mathrm{e}^{\sigma s} + G_1(s)\big) = 0 . \tag{57}$$

stay in the left half complex plane.

Since $G_0(s) = 0$ (see $H_0(s)$ in (55)) is the characteristic equation for linearized human car-following model (10), it is necessary that the human-driven vehicles are plant stable. This is a reasonable requirement as they should be able to maintain a desired speed with no disturbance from the traffic. By setting $s = \mathrm{i}\Omega$, $\Omega \geq 0$ in $G_0(s) = 0$ we obtain the plant stability boundary for human-driven vehicles as

$$\begin{aligned} \alpha &= \frac{\Omega^2 \cos(\tau \Omega)}{N^*} , \\ \beta &= \Omega \sin(\tau \Omega) - \frac{\Omega^2 \cos(\tau \Omega)}{N^*} . \end{aligned} \tag{58}$$

And in the remainder of this paper we only consider human parameters α, β inside the plant stability region enclosed by (58) and $\alpha = 0$ (given by $G(0) = 0$); see the shading in Fig. 9.

For the remaining part of (57), we plug (73) in (55,56) and obtain

$$s^2 \mathrm{e}^{\sigma s} + (\alpha_{11} + \beta_{11}) s + \alpha_{11} N^* = 0 , \tag{59}$$

the characteristic equation for the CCC driving model. Due to the similarity between (59) and $G_0(s) = 0$, the plant stability boundary is the same as (58) but with α_{11} instead of α, β_{11} instead of β, and σ instead of τ. However, it is more desirable to present it in the (γ_1, γ_2)-plane. Thus, we plug (51) into (59), consider $s = \mathrm{i}\Omega$, $\Omega \geq 0$, and obtain the plant stability boundary for the CCC vehicle as

$$\begin{aligned} \gamma_1 &= \frac{\Omega^4 \cos^2(\sigma \Omega)}{(N^*)^2} , \\ \gamma_2 &= \Omega^2 \sin^2(\sigma \Omega) - \frac{\Omega^4 \cos^2(\sigma \Omega)}{(N^*)^2} - 2\Omega^2 \cos(\sigma \Omega) . \end{aligned} \tag{60}$$

Since the cost function (18) requires $\gamma_1 > 0$, $\gamma_2 > 0$, we only consider the first quadrant of the (γ_1, γ_2)-plane. In Fig. 6,

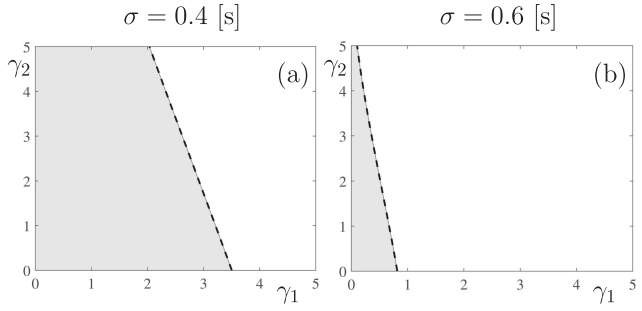

Fig. 6. Plant stability charts in the (γ_1, γ_2)-plane with communication delay σ as indicated. The plant stability boundaries are denoted by dashed black curves. The plant stable domains are shaded light gray.

the dashed curves represent plant stability boundaries, and the plant stability area is shaded as light gray for different values of communication delay as indicated. By comparing the two panels one may notice that as the communication delay increases the plant stable area shrinks, though it still covers a relatively large portion of the (γ_1, γ_2)-plane. Since the communication delay σ is seldom larger than human reaction time τ, panel (b) shows a quite conservative case.

B. Head-to-Tail String Stability

At the linear level the necessary and sufficient condition of head-to-tail string stability is given by

$$L(\omega) = |H(\mathrm{i}\omega)|^2 - 1 < 0\,, \quad \forall \omega > 0\,, \tag{61}$$

where $H(\mathrm{i}\omega)$ is defined by (54,55,56). String stability is violated when the maximum of $L(\omega)$ is larger than 0, and thus, the string stability boundary is given by the equations

$$L(\omega^{\mathrm{cr}}) = 0\,, \quad \frac{\partial L(\omega^{\mathrm{cr}})}{\partial \omega} = 0\,, \tag{62}$$

subject to $\dfrac{\partial^2 L(\omega^{\mathrm{cr}})}{\partial \omega^2} \leq 0$, where ω^{cr} indicates the location of the maximum of $L(\omega)$. When $\omega^{\mathrm{cr}} = 0$, we always have $L(0) = 0$, $\dfrac{\partial L(0)}{\partial \omega} = 0$, and the boundary is given by

$$\frac{\partial^2 L(0)}{\partial \omega^2} = 0\,. \tag{63}$$

As demonstrated in the previous section, feedback gains for vehicles i, $i > 6$ are negligibly small. Therefore we consider a connected vehicle system with $n = 5$. To obtain string stability charts, we solve (62) numerically and plot the string stability boundaries in the (γ_1, γ_2)-plane and in the (β, α)-plane for different values of communication delay and human reaction time.

The charts in Fig. 7 allow us to choose the design parameters γ_1, γ_2 so that head-to-tail string stability is ensured, as indicated by the dark gray region bounded by solid colored curves. The human gains are chosen as $\alpha = 0.6$ [1/s], $\beta = 0.9$ [1/s] and stability charts are shown for different values of human reaction time τ and communication delay σ. In the light gray region, only plant stability is satisfied. For the σ values considered here, all γ_1, γ_2 values in the windows shown ensure plant stability.

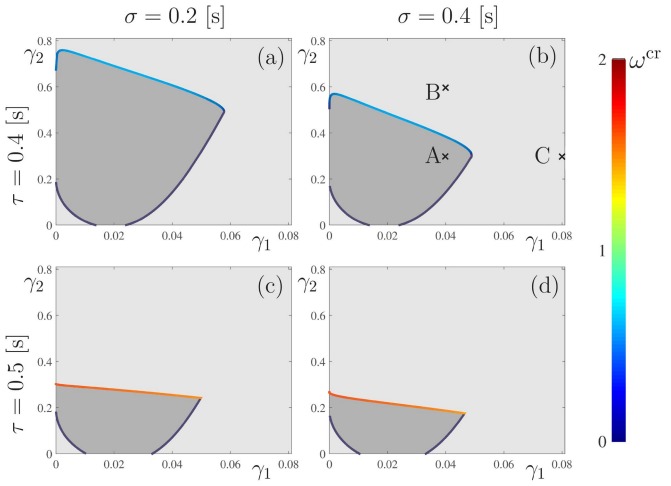

Fig. 7. Stability charts of a $(5 + 1)$-car platoon in the (γ_1, γ_2)-plane for human parameters $\alpha = 0.6$ [1/s], $\beta = 0.9$ [1/s]. The colored solid curves are the string stable boundaries. The coloring corresponds to the critical frequency at which string stability loss happens, as indicated by the colorbar on the right. Shading indicates plant stability while the string stable regions are shaded dark gray.

By comparing the size of the string stable region on the panels, we conclude that increasing the human reaction time and the communication delay both reduce string stability area, however, human reaction time affects the string stability more prominently. Notice that in order to achieve head-to-tail string stability, the weights γ_1, γ_2 have to be large enough. However, when either of these weights is exceedingly large, head-to-tail string stability will also be lost. The fact that both γ_1, γ_2 shall be below 1 to ensure string stability implies that penalties on velocity differences should be smaller than the penalty on the control effort (acceleration).

We remark that the human reaction time considered in Fig. 7 are larger than the critical reaction time $\tau_{\mathrm{cr}} \approx 0.325$ [s] and thus no string stability exists for any α, β combinations without V2V connectivity [17], but the system can be made head-to-tail string stable by using the connectivity in an appropriate way.

The coloring along the string stability boundaries shows the critical frequency where string stability loss happens, as indicated by the colorbar on the right. Red corresponds to higher frequency and blue corresponds to lower frequency. Leaving the string stable region through the dark blue curves, zero-frequency stability loss happens, while leaving it through the colored curve at the top, the stability loss happens at non-zero frequency, indicating the consequence of improper connectivity design.

To demonstrate string instabilities at different frequencies, we mark three points A, B, and C in Fig. 7(b) and plot the corresponding Bode plots in Fig. 8. Case A is string stable, with amplitude of transfer function smaller than 1 for all positive frequencies, cf. (61). The corresponding feedback gains and distribution kernels are given in Figs. 4 and 5. Case B has string instability in higher frequency range, due to the non-zero-frequency string stability loss at the boundary between points A and B. Such phenomenon has also been observed when using acceleration feedback in CCC

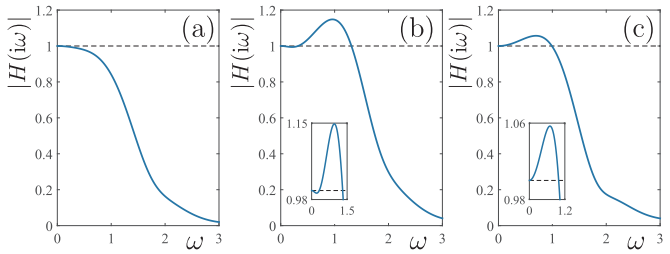

Fig. 8. Magnitude of transfer function as a function of the excitation frequency. Panels (a–c) correspond to points marked A–C in Fig. 7(a).

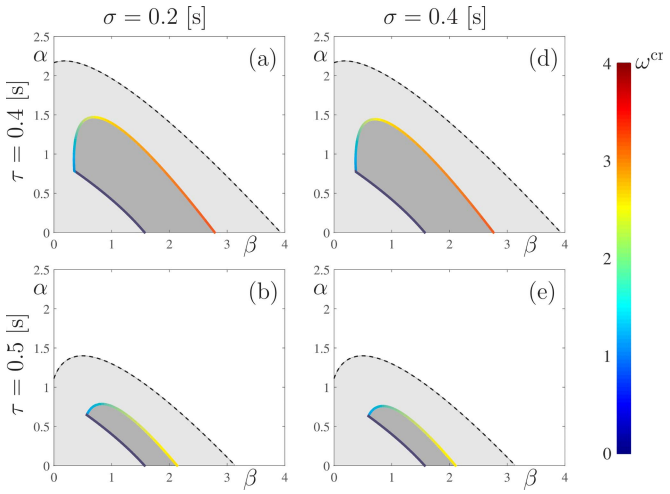

Fig. 9. Stability charts of a $(5+1)$-car platoon in the (β, α)-plane for design parameters $\gamma_1 = 0.01\,[1/s^2]$, $\gamma_2 = 0.10\,[1/s^2]$. The notation is the same as in Figs. 6 and 7.

design [19]. Case C is string unstable due to low-frequency instability, corresponding to the zero-frequency stability loss when crossing the boundary between points A and C.

The charts in Fig. 9 allows us to test the robustness of the CCC design for given design parameters with respect to different human parameters of the non-CCC vehicles. The same notations are used as in Figs. 6 and 7. The light gray areas bounded by black dashed curves given by (58) show the plant stable areas that shrink as human reaction time τ increases. The dark gray regions bounded by colored solid curves are string stable regions, with the color indicating the frequency at which the stability loss happens. The colors along the string stability boundaries show that both zero-frequency and non-zero-frequency string stability loss exists for all cases. Note that although there may be string stability regions outside the plant stability region, the lack of plant stability prevents the connected vehicle system from maintaining uniform traffic flow, so those regions are not shown in Fig. 9. Comparing the different panels in Fig. 9, we find that larger human reaction time significantly decreases the string stable area, while the communication delay only slightly deteriorates string stability.

V. Nonlinear Simulations

While the CCC controller is obtained with little computational cost using a linearized model for non-CCC vehicles, the algorithm should be able to accommodate nonlinearities arising in the dynamics of non-CCC vehicles, especially the nonlinearity in the range policy (3). Here we show that this nonlinearity can be added to the CCC design (49,53) by using the optimized feedback gains and distribution kernels. In particular, we can construct

$$
\begin{aligned}
\dot h_1(t) &= v_2(t) - v_1(t)\,,\\
\dot v_1(t) &= \sum_{i=1}^{n} \alpha_{1i}\big(V(h_i(t-\sigma)) - v_i(t-\sigma)\big)\\
&\quad + \sum_{i=1}^{n} \beta_{1i}\big(v_{i+1}(t-\sigma) - v_i(t-\sigma)\big)\\
&\quad + \sum_{i=1}^{n} \int_{-\tau}^{0} f_i(\theta)\big(V(h_i(t+\theta-\sigma)) - v_i(t+\theta-\sigma)\big)\mathrm{d}\theta\\
&\quad + \sum_{i=1}^{n} \int_{-\tau}^{0} g_i(\theta)\big(v_{i+1}(t+\theta-\sigma) - v_i(t+\theta-\sigma)\big)\mathrm{d}\theta,\\
\dot h_i(t) &= v_{i+1}(t) - v_i(t)\,,\\
\dot v_i(t) &= \alpha\big(V(h_i(t-\tau)) - v_i(t-\tau)\big) + \beta\big(v_{i+1}(t-\tau) - v_i(t-\tau)\big),
\end{aligned}
\tag{64}
$$

for $i = 2, \ldots, n$, cf. (1,2), whose linearization about the uniform flow equilibrium (6) is indeed (49,53).

To evaluate the performance at the nonlinear level, we consider a $(5 + 1)$-car system with human delay time $\tau = 0.4$ [s], communication delay $\sigma = 0.4$ [s] and simulate the propagation of headway and velocity perturbations along the connected vehicle system (64). The simulation is performed with Adam-Bashforth fourth-order method.

Fig. 10 compares the simulation results for the parameters corresponding to points A and B in Fig. 7(b) with the case where the CCC vehicle loses connectivity and has the same controller as the human-driven vehicles. The velocity profile of the head vehicle is $v_{n+1}(t) = v^* + v_{n+1}^{\mathrm{amp}} \sin(\omega t)$ with amplitude $v_{n+1}^{\mathrm{amp}} = 5$ [m/s], frequency $\omega = 1$ [rad/s] and $v^* = 15$ [m/s].

Without connectivity, attenuation of velocity perturbation is not possible as the human reaction time $\tau > \tau_{\mathrm{cr}}$. This is demonstrated by the black solid curve in Fig. 10(a). For the string unstable optimal design (point B in Fig. 7(b)), the velocity perturbation is attenuated as shown by the red solid curve in Fig. 10(a). However, the magnitude is still larger than that of the head vehicle (black dashed curve). On the other hand, for the string stable design corresponding to point A in Fig. 7(b), the CCC vehicle's velocity fluctuation (green solid curve) has smaller amplitude than the velocity input (black dashed curve), as depicted in Fig. 10(a). These results demonstrate that the linearized design can be used to predict the nonlinear behavior.

In Fig. 10(b), the headway fluctuations of the CCC vehicle (red and green solid curves) have smaller amplitude compared to the case without connectivity (black solid curve). This shows that although the CCC design is based on string stability in terms of velocity, the connectivity can also suppress headway errors. Notice that the headway fluctuation of the CCC vehicle in the string unstable case B (red solid curve) is slightly smaller than in the string stable case A (green solid curve), indicating a trade-off between attenuation of velocity and headway disturbances.

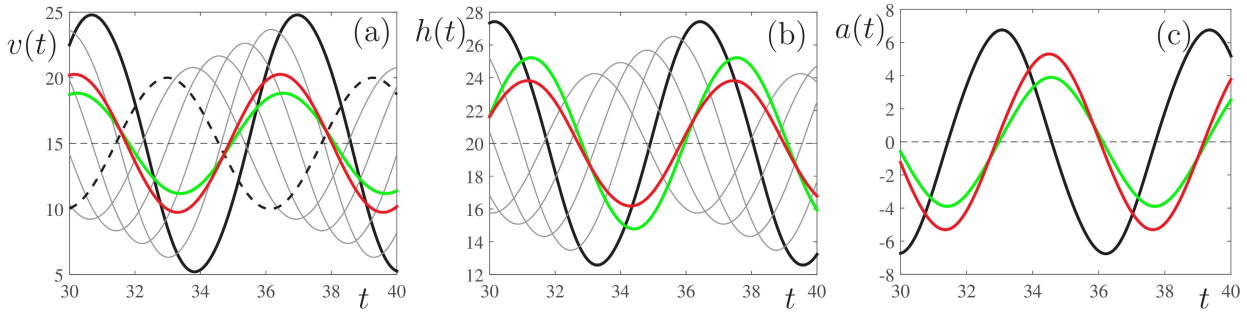

Fig. 10. Velocity, headway, and acceleration responses of a $(5+1)$-car vehicle string with human parameters $\alpha = 0.6[1/\mathrm{s}]$, $\beta = 0.9\,[1/\mathrm{s}]$, $\tau = 0.4$ [s] and communication delay $\sigma = 0.4$ [s]. The black solid curves represent the case with no connectivity when the tail vehicle is also human-driven. The green solid curves correspond to the string stable design of the CCC vehicle ($\gamma_1 = 0.04\,[1/\mathrm{s}^2]$, $\gamma_2 = 0.30\,[1/\mathrm{s}^2]$, see point A in Fig. 7(b)). The red solid curves correspond to the string unstable design of the CCC vehicle ($\gamma_1 = 0.04\,[1/\mathrm{s}^2]$, $\gamma_2 = 0.60\,[1/\mathrm{s}^2]$, see point B in Fig. 7(b)). The thin grey curves are for non-CCC vehicles, and the black dashed curve is the velocity perturbation of the head vehicle.

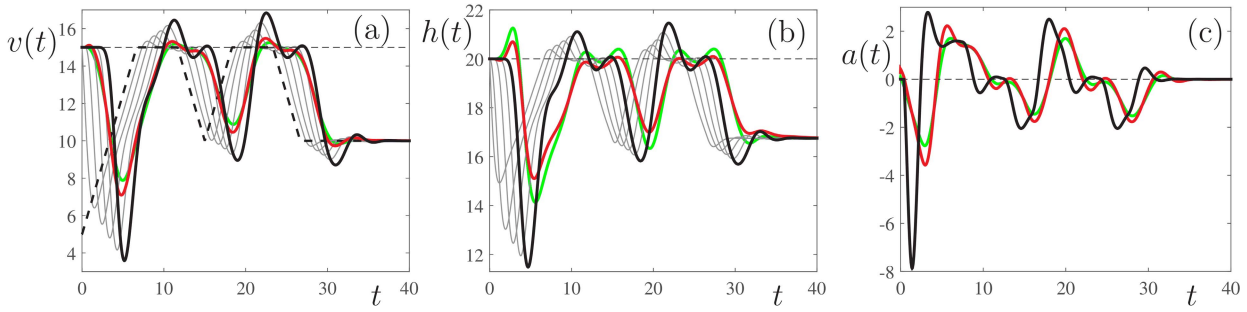

Fig. 11. Velocity, headway, and acceleration responses of a $(5+1)$-car vehicle string in a real-traffic scenario. Notations and parameters are the same as in Fig. 10.

In Fig. 10(c) the accelerations of the CCC vehicle (red and green solid curves) are significantly smaller compared with the case with no connectivity (black solid curve), where the acceleration gets excessively large. As the road surface and the vehicle powertrain are often not able to provide such large acceleration/deceleration, the vehicle in general may not be able to remain safe.

To test the proposed CCC controller in a more realistic traffic setting, we consider a velocity profile of the leading vehicle that contains deviations from the uniform flow with constant acceleration and a change of equilibrium points; see the black dashed curve in Fig. 11(a). Here we use the same parameters as in Fig. 10. Indeed, the velocity perturbation of the CCC vehicle is larger when a string unstable design is adopted (compare the red and green solid curves). However, even with string unstable design, the performance of CCC vehicles is still significantly better than if there was no connectivity (compare the red and the black solid curves). Especially that the acceleration response of the tail vehicle without connectivity (black solid curve) may exceed the limit of friction the road could provide, as it has to engage emergency maneuver for active safety. By exploiting the information of multiple vehicles ahead, CCC can be used to avoid such safety-critical situation.

VI. Conclusion

In this paper, we proposed a connected cruise control design based on linear quadratic regulation and analyzed the performance of the arising connected vehicle system where both automated and human-driven vehicles were allowed. By decomposing the optimization problem we showed that CCC can be designed sequentially as we incorporate signals from more and more vehicles ahead. Moreover, we showed that the gains decrease with the number of cars between the CCC vehicle and the signaling vehicle even when heterogeneity of human drivers is taken into account. This implies that a connected vehicle system using the proposed controller can gracefully degrade into smaller systems while maintaining certain optimality. Our analytical method significantly reduces the complexity of CCC design and is scalable for large connected vehicle systems.

We evaluated the head-to-tail string stability and summarized the results using stability charts. We showed that the optimized CCC is able to stabilize otherwise string unstable systems when the weights on the headway and velocity errors are chosen appropriately. Our design was also shown to be robust against variations of human parameters and was extended to the nonlinear level. The performance of our CCC strategy has been validated using numerical simulations. However, in order to be able to implement the results in real traffic scenarios experimental validation will be necessary which is left for future research.

Appendix

A. The Solution of LQR Problem With Delay

Here we present a detailed solution to the LQR problem with time delay. Since (20,21) is constructed to include

disturbance $\phi(t)$ in the LQR format, and the optimal controller (27) is given using partitioned matrices (26), we write (24,25) into four groups, where $\mathbf{P}_1(t)$, $\mathbf{Q}_1(t,\theta)$, $\mathbf{R}_1(t,\xi,\theta)$ are independent from the disturbance and can be solved using only the coefficient matrices $\mathbf{A}, \mathbf{B}, \mathbf{D}$ and the weighting factor Γ. That is, for the first group we obtain the PDE

$$\begin{aligned}
-\dot{\mathbf{P}}_1(t) &= \mathbf{A}^{\mathrm{T}}\mathbf{P}_1(t) + \mathbf{P}_1(t)\mathbf{A} - \mathbf{P}_1(t)\mathbf{D}\mathbf{D}^{\mathrm{T}}\mathbf{P}_1(t) \\
&\quad + \mathbf{Q}_1(t,0) + \mathbf{Q}_1^{\mathrm{T}}(t,0) + \mathbf{\Gamma}\,, \\
(\partial_\theta - \partial_t)\mathbf{Q}_1(t,\theta) &= \big(\mathbf{A}^{\mathrm{T}} - \mathbf{P}_1(t)\mathbf{D}\mathbf{D}^{\mathrm{T}}\big)\mathbf{Q}_1(t,\theta) + \mathbf{R}_1(t,0,\theta), \\
(\partial_\xi + \partial_\theta - \partial_t)\mathbf{R}_1(t,\xi,\theta) &= -\mathbf{Q}_1^{\mathrm{T}}(t,\xi)\mathbf{D}\mathbf{D}^{\mathrm{T}}\mathbf{Q}_1(t,\theta)\,, \qquad (65)
\end{aligned}$$

with boundary conditions

$$\begin{aligned}
&\mathbf{P}_1(t_{\mathrm{f}}) = \mathbf{0}\,, \\
&\mathbf{Q}_1(t_{\mathrm{f}},\theta) = \mathbf{0}\,, \qquad \mathbf{Q}_1(t,-\tau) = \mathbf{P}_1(t)\mathbf{B}\,, \\
&\mathbf{R}_1(t_{\mathrm{f}},\xi,\theta) = \mathbf{0}\,, \qquad \mathbf{R}_1(t,-\tau,\theta) = \mathbf{B}^{\mathrm{T}}\mathbf{Q}_1(t,\theta)\,. \qquad (66)
\end{aligned}$$

Using $\mathbf{P}_1(t)$ and $\mathbf{Q}_1(t,\theta)$ obtained from (65,66), we can calculate $\mathbf{Q}_2(t,\theta)$ and $\mathbf{R}_2(t,\xi,\theta)$ by solving

$$\begin{aligned}
(\partial_\theta - \partial_t)\mathbf{Q}_2(t,\theta) &= \big(\mathbf{A}^{\mathrm{T}} - \mathbf{P}_1(t)\mathbf{D}\mathbf{D}^{\mathrm{T}}\big)\mathbf{Q}_2(t,\theta) + \mathbf{R}_2(t,0,\theta), \\
(\partial_t - \partial_\xi - \partial_\theta)\mathbf{R}_2(t,\xi,\theta) &= \mathbf{Q}_1^{\mathrm{T}}(t,\xi)\mathbf{D}\mathbf{D}^{\mathrm{T}}\mathbf{Q}_2(t,\theta)\,, \qquad (67)
\end{aligned}$$

with boundary conditions

$$\begin{aligned}
&\mathbf{Q}_2(t_{\mathrm{f}},\theta) = \mathbf{0}\,, \qquad \mathbf{Q}_2(t,-\tau) = \mathbf{0}\,, \\
&\mathbf{R}_2(t_{\mathrm{f}},\xi,\theta) = \mathbf{0}\,, \qquad \mathbf{R}_2(t,-\tau,\theta) = \mathbf{B}^{\mathrm{T}}\mathbf{Q}_2(t,\theta)\,. \qquad (68)
\end{aligned}$$

Note that the disturbance $\phi(t)$ does not appear in (67) either. As a matter of fact, (67,68) result in $\mathbf{Q}_2(t,\theta) \equiv \mathbf{0}$ and $\mathbf{R}_2(t,\xi,\theta) \equiv \mathbf{0}$.

The dynamics of $\mathbf{P}_2(t)$ and $\mathbf{Q}_3(t,\theta)$ are driven by the disturbance $\phi(t)$:

$$\begin{aligned}
-\dot{\mathbf{P}}_2(t) &= \big(\mathbf{A}^{\mathrm{T}} - \mathbf{P}_1(t)\mathbf{D}\mathbf{D}^{\mathrm{T}}\big)\mathbf{P}_2(t) + \mathbf{P}_1(t)\phi(t) \\
&\quad + \mathbf{Q}_2(t,0) + \mathbf{Q}_3^{\mathrm{T}}(t,0)\,, \\
(\partial_\theta - \partial_t)\mathbf{Q}_3(t,\theta) &= \big(\phi^{\mathrm{T}}(t) - \mathbf{P}_2^{\mathrm{T}}(t)\mathbf{D}\mathbf{D}^{\mathrm{T}}\big)\mathbf{Q}_1(t,\theta) + \mathbf{R}_2^{\mathrm{T}}(t,\theta,0), \qquad (69)
\end{aligned}$$

with boundary conditions

$$\begin{aligned}
&\mathbf{P}_2(t_{\mathrm{f}}) = \mathbf{0}\,, \\
&\mathbf{Q}_3(t_{\mathrm{f}},\theta) = \mathbf{0}\,, \qquad \mathbf{Q}_3(t,-\tau) = \mathbf{P}_2^{\mathrm{T}}(t)\mathbf{B}\,. \qquad (70)
\end{aligned}$$

Although $\mathbf{P}_4(t)$, $\mathbf{Q}_4(t,\theta)$, $\mathbf{R}_4(t,\xi,\theta)$ do not appear in the optimal control (27), they appear in the minimal cost function, and are given by the PDE

$$\begin{aligned}
-\dot{\mathbf{P}}_4(t) &= \phi^{\mathrm{T}}(t)\mathbf{P}_2(t) + \mathbf{P}_3(t)\phi(t) - \mathbf{P}_3(t)\mathbf{D}\mathbf{D}^{\mathrm{T}}\mathbf{P}_2(t) \\
&\quad + \mathbf{Q}_4(t,0) + \mathbf{Q}_4^{\mathrm{T}}(t,0)\,, \\
(\partial_\theta - \partial_t)\mathbf{Q}_4(t,\theta) &= \big(\phi^{\mathrm{T}}(t) - \mathbf{P}_3(t)\mathbf{D}\mathbf{D}^{\mathrm{T}}\big)\mathbf{Q}_2(t,\theta) \\
&\quad + \mathbf{R}_4(t,0,\theta), \\
(\partial_\xi + \partial_\theta - \partial_t)\mathbf{R}_4(t,\xi,\theta) &= -\mathbf{Q}_2^{\mathrm{T}}(t,\xi)\mathbf{D}\mathbf{D}^{\mathrm{T}}\mathbf{Q}_2(t,\theta)\,, \qquad (71)
\end{aligned}$$

with boundary conditions

$$\begin{aligned}
&\mathbf{P}_4(t_{\mathrm{f}}) = \mathbf{0}\,, \\
&\mathbf{Q}_4(t_{\mathrm{f}},\theta) = \mathbf{0}\,, \qquad \mathbf{Q}_4(t,-\tau) = \mathbf{0}\,, \\
&\mathbf{R}_4(t_{\mathrm{f}},\xi,\theta) = \mathbf{0}\,, \qquad \mathbf{R}_4(t,-\tau,\theta) = \mathbf{0}\,. \qquad (72)
\end{aligned}$$

B. The Distribution Kernels

Here we provide the constants that appear in the expression of $f_i(\theta), g_i(\theta), i = 1,\ldots,n$ in (50) using (44,48,52). For $i = 1$ (52) corresponds to

$$a_{10} = a_{11} = a_{12} = 0, \quad b_{10} = b_{11} = b_{12} = 0\,. \qquad (73)$$

For $i = 2,\ldots,n$ we write in (44) that

$$\mathrm{e}^{\hat{\mathbf{A}}_1(\theta+\tau)} = \mathbf{K}\mathrm{e}^{\hat{\mathbf{J}}_1(\theta+\tau)}\mathbf{K}^{-1}\,, \qquad (74)$$

where the Jordan form $\hat{\mathbf{J}}_1$ contains the eigenvalues of $\hat{\mathbf{A}}_1$:

$$\lambda_{1,2} = \frac{1}{2}\Big(-\sqrt{\gamma_1+\gamma_2+2N^*\sqrt{\gamma_1}} \pm \sqrt{\gamma_1+\gamma_2-2N^*\sqrt{\gamma_1}}\Big)\,, \qquad (75)$$

and the real part of λ_1, λ_2 are smaller than zero (which is ensured by the closed-loop plant stability of LQ design). In most cases $\hat{\mathbf{A}}_1$ is diagonalizable, that is, $\hat{\mathbf{J}}_1 = \mathrm{diag}([\lambda_1, \lambda_2])$. In the special case $\gamma_2 = 2N^*\sqrt{\gamma_1} - \gamma_1$, we have $\lambda_1 = \lambda_2$ and $\hat{\mathbf{A}}_1$ may not be diagonalizable, yielding the nontrivial Jordan form $\hat{\mathbf{J}}_1 = \begin{bmatrix}\lambda_1 & 1\\ 0 & \lambda_1\end{bmatrix}$.

Denote $\mathbf{K} = \begin{bmatrix}k_{11} & k_{12}\\ k_{21} & k_{22}\end{bmatrix}$, $\mathbf{K}^{-1} = \begin{bmatrix}i_{11} & i_{12}\\ i_{21} & i_{22}\end{bmatrix}$, then from (44,48) we obtain

$$\big[f_i(\theta)\; g_i(\theta)\big] = \big[f_{\mathrm{c}}(\theta)\; g_{\mathrm{c}}(\theta)\big]\big(\mathbf{P}_{1i}\mathbf{B}_1 + \mathbf{P}_{1(i-1)}\mathbf{B}_2\big), \qquad (76)$$

where

$$\begin{aligned}
f_{\mathrm{c}}(\theta) &= \big(t_{\mathrm{ca}} + t_{\mathrm{cc}}(\theta+\tau)\big)\mathrm{e}^{\lambda_1(\theta+\tau)} + t_{\mathrm{cb}}\mathrm{e}^{\lambda_2(\theta+\tau)}\,, \\
g_{\mathrm{c}}(\theta) &= \big(s_{\mathrm{ca}} + s_{\mathrm{cc}}(\theta+\tau)\big)\mathrm{e}^{\lambda_1(\theta+\tau)} + s_{\mathrm{cb}}\mathrm{e}^{\lambda_2(\theta+\tau)}\,, \qquad (77)
\end{aligned}$$

such that we have

$$\begin{aligned}
t_{\mathrm{ca}} &= (k_{11}+k_{21})i_{11}\,, \qquad t_{\mathrm{cb}} = (k_{12}+k_{22})i_{21}\,, \\
s_{\mathrm{ca}} &= (k_{11}+k_{21})i_{12}\,, \qquad s_{\mathrm{cb}} = (k_{12}+k_{22})i_{22}\,, \\
t_{\mathrm{cc}} &= \begin{cases} 0\,, & \text{if } \hat{\mathbf{A}}_1 \text{ is diagonalizable}\,, \\ (k_{11}+k_{21})i_{21}\,, & \text{if } \hat{\mathbf{A}}_1 \text{ is not diagonalizable}\,, \end{cases} \\
s_{\mathrm{cc}} &= \begin{cases} 0\,, & \text{if } \hat{\mathbf{A}}_1 \text{ is diagonalizable}\,, \\ (k_{11}+k_{21})i_{22}\,, & \text{if } \hat{\mathbf{A}}_1 \text{ is not diagonalizable}\,. \end{cases} \qquad (78)
\end{aligned}$$

Substituting (17,77) into (76), we obtain (50) with the coefficients

$$\begin{aligned}
a_{i0} &= \alpha(t_{\mathrm{ca}}l_{i1} + s_{\mathrm{ca}}l_{i2})\,, \qquad b_{i0} = \beta(t_{\mathrm{ca}}l_{i1} + s_{\mathrm{ca}}l_{i2})\,, \\
a_{i1} &= \alpha(t_{\mathrm{cc}}l_{i1} + s_{\mathrm{cc}}l_{i2})\,, \qquad b_{i1} = \beta(t_{\mathrm{cc}}l_{i1} + s_{\mathrm{cc}}l_{i2})\,, \\
a_{i2} &= \alpha(t_{\mathrm{cb}}l_{i1} + s_{\mathrm{cb}}l_{i2})\,, \qquad b_{i2} = \beta(t_{\mathrm{cb}}l_{i1} + s_{\mathrm{cb}}l_{i2})\,, \qquad (79)
\end{aligned}$$

where

$$\begin{aligned}
l_{i1} &= -\mathbf{P}_{1i}[1,1] - \mathbf{P}_{1i}[1,2] + \mathbf{P}_{1(i-1)}[1,2]\,, \\
l_{i2} &= -\mathbf{P}_{1i}[2,1] - \mathbf{P}_{1i}[2,2] + \mathbf{P}_{1(i-1)}[2,2]\,, \qquad (80)
\end{aligned}$$

for $i = 2,\ldots,n$, and $\mathbf{C}[i,j]$ stands for the element of $\mathbf{C}$ at the i^{th} row and j^{th} column.

C. The Contracting Map

To show that the feedback gains and distribution functions decay exponentially with the car number, all eigenvalues of $\mathbf{M}$ must be smaller than 1 in magnitude, cf. (46,47).

We assume diagonalizable $\hat{\mathbf{A}}_1$ and plug (74) into (47) to obtain

$$\mathbf{M} = (\mathbf{I}\otimes\mathbf{K})\tilde{\mathbf{M}}(\mathbf{I}\otimes\mathbf{K}^{-1}), \tag{81}$$

where

$$\tilde{\mathbf{M}} = -\begin{bmatrix} \hat{\mathbf{J}}_1 - \alpha e^{\tau\hat{\mathbf{J}}_1} & -\alpha e^{\tau\hat{\mathbf{J}}_1} \\ N^*\mathbf{I} - \beta e^{\tau\hat{\mathbf{J}}_1}\hat{\mathbf{J}}_1 & -\beta e^{\tau\hat{\mathbf{J}}_1} \end{bmatrix}^{-1} \begin{bmatrix} \mathbf{0} & \alpha e^{\tau\hat{\mathbf{J}}_1} \\ \mathbf{0} & \beta e^{\tau\hat{\mathbf{J}}_1} \end{bmatrix}. \tag{82}$$

Indeed, the eigenvalues of $\mathbf{M}$ are the same as the eigenvalues of $\tilde{\mathbf{M}}$. It is evident that $\tilde{\mathbf{M}}$ has two zero eigenvalues, while the other two non-zero eigenvalues are

$$\mu_{1,2} = -\frac{\alpha N^* - \beta\lambda_{1,2}}{\lambda_{1,2}^2 e^{-\tau\lambda_{1,2}} - (\alpha+\beta)\lambda_{1,2} + \alpha N^*}, \tag{83}$$

where $\lambda_{1,2}$ are given in (75). That is, the recursive map (46,47) is contracting if

$$|\mu_1| < 1, \quad |\mu_2| < 1. \tag{84}$$

Consider plant stable human-driven vehicles where N^* and α, β are positive. We found that (84) holds in the string stable region in the parameter space. Note that (83) bears an interesting resemblance to $H_0(s)$ in (55), and still holds when $\hat{\mathbf{A}}_1$ is not diagonalizable.

D. Robustness of CCC Against Other CCC Vehicles

Here we consider the scenario where vehicles $2-n$ in Fig. 2 are no longer homogeneous, that is, some of them may have different human parameters or even become CCC vehicles. To demonstrate the general influence of heterogeneity among preceding vehicles on the CCC design, we assume the dynamics of vehicle i is

$$\begin{aligned} \dot{h}_i(t) &= v_{i+1}(t) - v_i(t), \\ \dot{v}_i(t) &= \sum_{j=i}^{n}\Big(\alpha_{ij}\big(V_j(h_j(t-\tau)) - v_j(t-\tau)\big) + \beta_{ij}\,\dot{h}_j(t-\tau)\Big), \end{aligned} \tag{85}$$

for $i = 2,\dots,n$, where α_{ij}, β_{ij} are vehicle i's feedback gains on motion signals from vehicle j, cf. (2,64).

Thus, the dynamics of the connected vehicle system is still described by (15), with a new coefficient matrix

$$\mathbf{B} = \begin{bmatrix} \mathbf{0} & \mathbf{B}_{12} & \mathbf{B}_{13} & \cdots & \mathbf{B}_{1n} \\ & \mathbf{B}_{22} & \mathbf{B}_{23} & \cdots & \mathbf{B}_{2n} \\ & & \ddots & & \vdots \\ & & & \mathbf{B}_{(n-1)(n-1)} & \mathbf{B}_{(n-1)n} \\ & & & & \mathbf{B}_{nn} \end{bmatrix}, \tag{86}$$

where

$$\begin{aligned} \mathbf{B}_{1i} &= \begin{bmatrix} 0 & 0 \\ \alpha_{2i} & \beta_{2i} \end{bmatrix}, \quad \mathbf{B}_{ii} = -\begin{bmatrix} \alpha_{ii} & \beta_{ii} \\ \alpha_{ii} & \beta_{ii} \end{bmatrix}, \quad i = 2,\cdots,n, \\ \mathbf{B}_{ij} &= \begin{bmatrix} -\alpha_{ij} & -\beta_{ij} \\ \alpha_{(i+1)j} - \alpha_{ij} & \beta_{(i+1)j} - \beta_{ij} \end{bmatrix}, \quad j = i+1,\cdots,n, \end{aligned} \tag{87}$$

cf. (16,17).

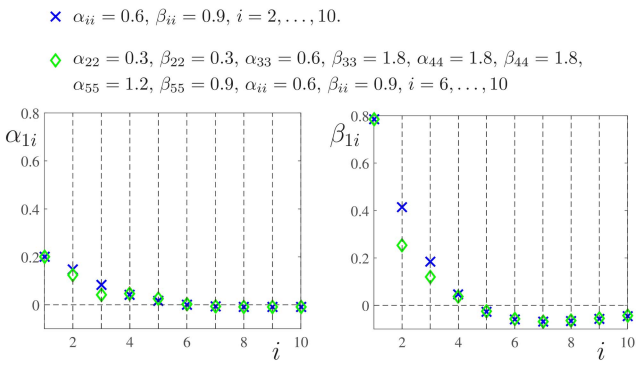

Fig. 12. The optimized headway and velocity gains $\alpha_{1i}, \beta_{1i}, i = 1,\dots,n$ of the CCC vehicle in a $(10+1)$-car system for homogeneous (blue crosses) and heterogeneous (green diamonds) human gains as indicated. The other parameters are the same as in Fig. 4.

Since the matrix $\mathbf{B}$ is still upper-triangular, the optimal control design (31,32,34) can be decomposed as before. Now instead of (44,46,47), we have

$$\mathbf{Q}_{1i}(\theta) = \sum_{k=1}^{i} e^{\hat{\mathbf{A}}_1(\theta+\tau)}\mathbf{P}_{1k}\mathbf{B}_{ki}, \tag{88}$$

and

$$\mathrm{vec}(\mathbf{P}_{1i}) = \sum_{k=1}^{i-1}\mathbf{M}_{ik}\,\mathrm{vec}(\mathbf{P}_{1k}), \tag{89}$$

for $i = 2,\dots,n$, where

$$\mathbf{M}_{ik} = -(\mathbf{I}\otimes\hat{\mathbf{A}}_1 + \mathbf{A}_1^{\mathrm{T}}\otimes\mathbf{I} + \mathbf{B}_{ii}^{\mathrm{T}}\otimes e^{\tau\hat{\mathbf{A}}_1})^{-1}(\mathbf{B}_{ki}^{\mathrm{T}}\otimes e^{\tau\hat{\mathbf{A}}_1}). \tag{90}$$

This means that the maps between $\mathrm{vec}(\mathbf{P}_{1i})$, $i = 2,\dots,n$, and $\mathrm{vec}(\mathbf{P}_{11})$ are determined by $\mathbf{B}_{ki}$, $k = 2,\dots,i-1$, i.e., by the connectivity structure between vehicle 1 and vehicle i. Thus, the connectivity structure among vehicles farther downstream still does not influence feedback gains on existing feedback terms of the CCC controller.

We first demonstrate only the influence of heterogeneous human parameters. In this case, the coefficient matrix $\mathbf{B}$ still has the same structure is in (16), i.e., $\mathbf{B}_{ij} \neq \mathbf{0}$ only for $j = i+1$. Thus, there is only one term $\mathbf{M}_{i(i-1)}$ left in the right-hand side of (89), and it still defines a recursively contracting map given plant stable human parameters in (90).

As an example, we take a $(10+1)$-car connected system, keep the design parameters $\gamma_1 = 0.04\,[1/\mathrm{s}^2]$, $\gamma_2 = 0.30\,[1/\mathrm{s}^2]$ and human reaction time $\tau = 0.4$ [s] as in Fig. 4, but increase/decrease the human gains for vehicles $2,3,4,5$ as indicated in Fig. 12. The blue crosses correspond to the homogeneous system (cf. Fig. 4), while the green diamonds correspond to the heterogeneous system. The gains α_{11}, β_{11} are the same for both cases, because they do not depend on parameters of preceding vehicles. Although α_{1i}, β_{1i}, $i = 2,\dots,n$ differ between the homogeneous and heterogeneous cases, the difference is only noticeable for $i = 2,3$, even though α_{44}, β_{44}, α_{55}, β_{55} differ significantly. This is because the contracting map (89,90) forces the gains to

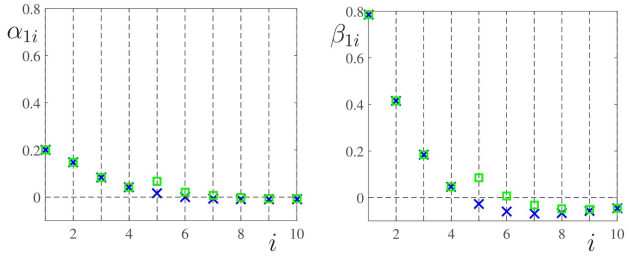

Fig. 13. The optimized headway and velocity gains $\alpha_{1i}, \beta_{1i}, i = 2, \ldots, n$ of the CCC vehicle in a $(10+1)$-car connected vehicle system. The blue crosses denote gains obtained with homogeneous human-driven vehicles, while the green squares denote the case when vehicle 3 uses additional feedback from vehicle 5, with gains $\alpha_{35} = 0.9\,[1/\mathrm{s}]$ and $\beta_{35} = 0.9\,[1/\mathrm{s}]$. The other parameters are the same as in Fig. 4.

decrease for signals coming from farther downstream, and then heterogeneity of vehicles further away has less significant impact on the CCC vehicle.

We then consider the robustness of the CCC design against extra connectivity links among preceding vehicles. In Fig. 13, the blue crosses still show the gains in a $(10+1)$-car system with homogeneous human-driven vehicles (cf. Fig. 4), while the green squares depict the case when vehicle 3 is also using motion information of vehicle 5, with feedback gains $\alpha_{35} = 0.6\,[1/\mathrm{s}]$ and $\beta_{35} = 0.9\,[1/\mathrm{s}]$. Notice that the gains α_{1i}, β_{1i} of the CCC controller do not change for $i = 1, \ldots, 4$. While α_{15} and β_{15} change considerably, as i increases further the changes in α_{1i}, β_{1i} decay exponentially. These case studies demonstrate that our proposed algorithm is robust against heterogeneity among preceding vehicles.

REFERENCES

[1] D. Schrank, B. Eisele, and T. Lomax, "TTI's 2012 urban mobility report," Texas A&M Transp. Inst. and Texas A&M Univ. Syst., College Station, TX, USA, 2012.

[2] K. Li and P. Ioannou, "Modeling of traffic flow of automated vehicles," *IEEE Trans. Intell. Transp. Syst.*, vol. 5, no. 2, pp. 99–113, Jun. 2004.

[3] L. C. Davis, "Effect of adaptive cruise control systems on traffic flow," *Phys. Rev. E*, vol. 69, no. 6, p. 066110, Jun. 2004.

[4] X. Cheng, L. Yang, and X. Shen, "D2D for intelligent transportation systems: A feasibility study," *IEEE Trans. Intell. Transp. Syst.*, vol. 16, no. 4, pp. 1784–1793, Aug. 2015.

[5] X. Cheng *et al.*, "Electrified vehicles and the smart grid: The ITS perspective," *IEEE Trans. Intell. Transp. Syst.*, vol. 15, no. 4, pp. 1388–1404, Aug. 2014.

[6] E. V. Nunen, M. R. J. A. E. Kwakkernaat, J. Ploeg, and B. D. Netten, "Cooperative competition for future mobility," *IEEE Trans. Intell. Transp. Syst.*, vol. 13, no. 3, pp. 1018–1025, Sep. 2012.

[7] E. Chan, P. Gilhead, P. Jelínek, P. Krejčí, and T. Robinson, "Cooperative control of SARTRE automated platoon vehicles," in *Proc. 19th ITS World Congr.*, 2012, pp. 22–26.

[8] B. van Arem, C. J. G. van Driel, and R. Visser, "The impact of cooperative adaptive cruise control on traffic-flow characteristics," *IEEE Trans. Intell. Transp. Syst.*, vol. 7, no. 4, pp. 429–436, Dec. 2006.

[9] M. di Bernardo, A. Salvi, and S. Santini, "Distributed consensus strategy for platooning of vehicles in the presence of time-varying heterogeneous communication delays," *IEEE Trans. Intell. Transp. Syst.*, vol. 16, no. 1, pp. 102–112, Feb. 2015.

[10] V. Milanes, J. Alonso, L. Bouraoui, and J. Ploeg, "Cooperative maneuvering in close environments among cybercars and dual-mode cars," *IEEE Trans. Intell. Transp. Syst.*, vol. 12, no. 1, pp. 15–24, Mar. 2011.

[11] J. Ploeg, N. van de Wouw, and H. Nijmeijer, "$\mathcal{L}_p$ string stability of cascaded systems: Application to vehicle platooning," *IEEE Trans. Control Syst. Technol.*, vol. 22, no. 2, pp. 786–793, Mar. 2014.

[12] J. Ploeg, E. Semsar-Kazerooni, G. Lijster, N. van de Wouw, and H. Nijmeijer, "Graceful degradation of cooperative adaptive cruise control," *IEEE Trans. Intell. Transp. Syst.*, vol. 16, no. 1, pp. 488–497, Feb. 2015.

[13] J. Ploeg, D. P. Shukla, N. van de Wouw, and H. Nijmeijer, "Controller synthesis for string stability of vehicle platoons," *IEEE Trans. Intell. Transp. Syst.*, vol. 15, no. 2, pp. 845–865, Apr. 2014.

[14] M. Wang, W. Daamen, S. P. Hoogendoorn, and B. van Arem, "Rolling horizon control framework for driver assistance systems. Part II: Cooperative sensing and cooperative control," *Transp. Res. C*, vol. 40, pp. 290–311, Mar. 2014.

[15] Y. Zheng, S. E. Li, J. Wang, D. Cao, and K. Li, "Stability and scalability of homogeneous vehicular platoon: Study on the influence of information flow topologies," *IEEE Trans. Intell. Transp. Syst.*, vol. 17, no. 1, pp. 14–26, Jan. 2016.

[16] G. Orosz, "Connected cruise control: Modelling, delay effects, and nonlinear behaviour," *Vehicle Syst. Dyn.*, vol. 54, no. 8, pp. 1147–1176, 2016.

[17] L. Zhang and G. Orosz, "Motif-based design for connected vehicle systems in presence of heterogeneous connectivity structures and time delays," *IEEE Trans. Intell. Transp. Syst.*, vol. 17, no. 6, pp. 1638–1651, Jun. 2016.

[18] G. Orosz, R. E. Wilson, and G. Stépán, "Traffic jams: Dynamics and control," *Philos. Trans. Roy. Soc. A*, vol. 368, no. 1928, pp. 4455–4479, 2010.

[19] J. I. Ge and G. Orosz, "Dynamics of connected vehicle systems with delayed acceleration feedback," *Transp. Res. C, Emerg. Technol.*, vol. 46, pp. 46–64, Sep. 2014.

[20] W. B. Qin, M. M. Gomez, and G. Orosz, "Stability and frequency response under stochastic communication delays with applications to connected cruise control design," *IEEE Trans. Intell. Transp. Syst.*, vol. PP, no. 99, pp. 1–16. [Online]. Available: http://dx.doi.org/10.1109/TITS.2016.2574246

[21] S. S. Avedisov and G. Orosz, "Nonlinear network modes in cyclic systems with applications to connected vehicles," *J. Nonlinear Sci.*, vol. 25, no. 4, pp. 1015–1049, Aug. 2015.

[22] J. I. Ge and G. Orosz, "Optimal control of connected vehicle systems," in *Proc. 53rd IEEE Conf. Decision Control*, Dec. 2014, pp. 4107–4112.

[23] D. Helbing, "Traffic and related self-driven many-particle systems," *Rev. Mod. Phys.*, vol. 73, no. 4, pp. 1067–1141, 2001.

[24] K. Nagel, P. Wagner, and R. Woesler, "Still flowing: Approaches to traffic flow and traffic jam modeling," *Oper. Res.*, vol. 51, no. 5, pp. 681–710, 2003.

[25] M. Treiber, A. Hennecke, and D. Helbing, "Congested traffic states in empirical observations and microscopic simulations," *Phys. Rev. E*, vol. 62, no. 2, pp. 1805–1824, 2000.

[26] M. Bando, K. Hasebe, A. Nakayama, A. Shibata, and Y. Sugiyama, "Dynamical model of traffic congestion and numerical simulation," *Phys. Rev. E*, vol. 51, pp. 1035–1042, Feb. 1995.

[27] R. Herman, E. W. Montroll, R. B. Potts, and R. W. Rothery, "Traffic dynamics: Analysis of stability in car following," *Oper. Res.*, vol. 7, no. 1, pp. 86–106, 1959.

[28] D. C. Gazis, R. Herman, and R. W. Rothery, "Nonlinear follow-the-leader models of traffic flow," *Oper. Res.*, vol. 9, no. 4, p. 545–567, 1961.

[29] P. A. Ioannou and M. Stefanovic, "Evaluation of ACC vehicles in mixed traffic: Lane change effects and sensitivity analysis," *IEEE Trans. Intell. Transp. Syst.*, vol. 6, no. 1, pp. 79–89, Mar. 2005.

[30] S. Krauss, P. Wagner, and C. Gawron, "Metastable states in a microscopic model of traffic flow," *Phys. Rev. E*, vol. 55, no. 5, pp. 5597–5602, 1997.

[31] R. Wiedemann, *Simulation des Strassenverkehrsflusses* (Institut Fur Verkehrswesen Der). Karlsruhe, Germany: Univ. Karlsruhe, 1973.

[32] D. Krajzewicz, J. Erdmann, M. Behrisch, and L. Bieker, "Recent development and applications of SUMO—Simulation of urban mobility," *Int. J. Adv. Syst. Meas.*, vol. 5, nos. 3–4, pp. 128–138, 2012.

[33] Q. Yang and H. N. Koutsopoulos, "A microscopic traffic simulator for evaluation of dynamic traffic management systems," *Transp. Res. C, Emerg. Technol.*, vol. 4, no. 3, pp. 113–129, Jun. 1996.

[34] S. Hoogendoorn and R. Hoogendoorn, "Calibration of microscopic traffic-flow models using multiple data sources," *Philos. Trans. Roy. Soc. London A, Math. Phys. Sci.*, vol. 368, no. 1928, pp. 4497–4517, 2010.

[35] P. Wagner, "Fluid-dynamical and microscopic description of traffic flow: A data-driven comparison," *Philos. Trans. Roy. Soc. London A, Math. Phys. Sci.*, vol. 368, no. 1928, pp. 4481–4495, 2010.

[36] P. Seiler, A. Pant, and K. Hedrick, "Disturbance propagation in vehicle strings," *IEEE Trans. Autom. Control*, vol. 49, no. 10, pp. 1835–1842, Oct. 2004.
[37] C. R. He, H. Maurer, and G. Orosz, "Fuel consumption optimization of heavy-duty vehicles with grade, wind, and traffic information," *J. Comput. Nonlinear Dyn.*, vol. 11, no. 6, p. 061011-1–061011-12, 2016.
[38] V. Kolmanovskii and A. Myshkis, *Applied Theory of Functional Differential Equations*. Norwell, MA, USA: Kluwer, 1992.
[39] D. W. Ross and I. Flügge-Lotz, "An optimal control problem for systems with differential-difference equation dynamics," *J. Control*, vol. 7, no. 4, pp. 609–623, 1969.
[40] F. Bai and H. Krishnan, "Reliability analysis of DSRC wireless communication for vehicle safety applications," in *Proc. IEEE Intell. Transp. Syst. Conf.*, Sep. 2006, pp. 355–362.

Jin I. Ge received the bachelor's degree in transportation engineering and the master's degree in automotive engineering from Beijing University of Aeronautics and Astronautics, China, in 2010 and 2012, respectively. She is currently working toward the Ph.D. degree in mechanical engineering with University of Michigan, Ann Arbor. Her research focuses on dynamics and control of connected vehicles, optimal control, and time delay systems.

Gábor Orosz received the M.Sc. degree in engineering physics from Budapest University of Technology and Economics, Hungary, in 2002 and the Ph.D. degree in engineering mathematics from University of Bristol in 2006. He held postdoctoral positions with University of Exeter and University of California, Santa Barbara. He has been an Assistant Professor in mechanical engineering with University of Michigan, Ann Arbor, since 2010. His research focuses on nonlinear dynamics and control, time delay systems, networks and complex systems with applications on connected and automated vehicles, and biological networks.